NASA-CR-194118

FINAL REPORT

NASA GRANT NSG 5386

ANALYSIS OF THE IUE SPECTRA OF THE STRONGLY INTERACTING BINARY BETA LYRAE

for

ARCHIVAL RESEARCH PROGRAM

INTERNATIONAL ULTRAVIOLET EXPLORER

Principle Investigator: Dr. George E. McCluskey, Jr.
Division of Astronomy
Department of Mathematics
Lehigh University
14 East Packer Avenue
Bethlehem, PA 18015

NASA Technical Officer: Dr. Yoji Kondo
Code 684
Laboratory for Astronomy and Solar Physics
Space Sciences Directorate
NASA Goddard Space Flight Center
Greenbelt, MD 20771

(NASA-CR-194118) ANALYSIS OF THE IUE SPECTRA OF THE STRONGLY INTERACTING BINARY BETA LYRAE Final Report (Lehigh Univ.) 54 p

N94-14493

Unclas

G3/89 0182914

Ultraviolet Light Curves of Beta Lyrae: Comparison of OAO-A2, IUE and Voyager Observations

by

Yoji Kondo[1], George E. McCluskey[2], Jeffrey M.S. Silvis[3], Ronald S. Polidan[1], Carolina P.S. McCluskey[4], Joel A. Eaton[5]

ABSTRACT

The six-band ultraviolet light curves of beta Lyrae obtained with the Orbiting Astronomical Observatory A-2 in 1970 exhibited a very unusual behavior. The secondary minimum deepened at shorter wavelength, indicating that one was not observing light variations caused primarily by the eclipses of two stars having a roughly Planckian energy distribution. It was then suggested that the light variations were caused by a viewing angle effect of an optically-thick, ellipsoidal circumbinary gas cloud. Since 1978 beta Lyrae has been observed with the International Ultraviolet Explorer (IUE) satellite. We have constructed

---

1. NASA Goddard Space Flight Center
2. Lehigh University
3. The Catholic University of America
4. Pennsylvania State University
5. Tennessee State University

ultraviolet light curves from the IUE archival data for comparison with the OAO-A2 results. We find that they are in substantial agreement with each other. The Voyager ultraviolet spectrometer was also used to observe this binary during a period covered by IUE observations. The Voyager results agree with those of the two other satellite observatories at wavelengths longer than about 1350 A. However, in the wavelength region shorter than the Lyman-alpha line at 1216 A, the light curves at 1085 A and 965 A show virtually no light variation except an apparent flaring near phase 0.7, which is also in evidence at longer wavelengths. We suggest that the optically-thick circumbinary gas cloud, which envelops the two stars completely, assumes a roughly spherical shape when observed at these shorter wavelengths.

I. OBSERVATIONS

A. OAO-A2 Observations

The Orbiting Astronomical Observatory (OAO) A-2 observations were obtained consecutively for 15 days - from 1970 October 27 to November 13 - using the Wisconsin instruments on board. Photometers with pass-bands centered at 3320, 1910, and 1430 A and at 2980, 2450, and 1550 A were used on alternate orbits. More details and appropriate citations for the OAO-A2 instruments and observations were given in the earlier papers (Kondo, McCluskey and Houck 1971, 1972; Kondo, McCluskey and Eaton 1976). Figures 1a-1e give the OAO-A2 light curves, plotted with the IUE light curves for comparison, Table 1 the OAO-A2 observations, and Table 2 the characteristics for the filters used.

The light elements used for computing the phases for Table 1 and Figure 1 OAO-A2 light curves were from the ephemeris by Wood and Forbes (1973). The orbital period of this binary continues to change, due to the mass flow within and out of the binary system. The OAO-A2 observations were obtained continuously in 1970 during one orbit so that any slight change in computed phases would only shift the light curve in toto along the phase axis. Consequently, it was decided <u>not</u> to recompute the phases using the more recent light elements, which were used to compute the phases for the IUE and Voyager observations.

B. IUE Observations.

The IUE observations were obtained over a period of eight years.

For comparisons with the OAO-A2 results, we have integrated the flux over somewhat arbitrarily chosen segments of the spectra; before the choice of the central wavelength was made, we had ascertained that it was not centered at a recognizable absorption or emission feature within a few angstroms from the bin center. The spectral bands chosen are 10, 50, 70 and 100 A, which are centered at wavelengths 1250, 1365, 1430, 1570, 1726, and 1835 A in the far-ultraviolet (IUE SWP camera) and at 2180, 2470, 2720 and 2980 A in the mid-ultraviolet (IUE LWP camera). Some spectra are overexposed at the longest wavelengths in both cameras. In such cases, the overexposed data points have been removed from both the tables and the figures. Some exposures were made at low resolution (delta lambda = 6-7 A), while other spectra were obtained at high resolution (delta lambda = 0.1-0.3 A) but the results are so consistent with each other that we have plotted the low and high results on the same figures.

We note that to be photometrically accurate the low dispersion data must be taken with the large aperture. Most LWP camera images of this type had been overexposed by a factor of three and are not suitable for our analysis. No LWP low-dispersion spectra were included in this study. In the case of low dispersion SWP images, they were usually exposed for 2 seconds. But, a few had one second exposure times and these images deviated greatly from the light curves. The one second exposure spectra are probably strongly affected by the camera rise time, which is about 0.5 second; so these were also excluded.

The SWP camera's sensitivity has linearly decreased over the last ten years by about one percent per year. Observations of the stars tau Sco (HD149438) and lambda Lep (HD34816) were used to find the coefficients of a straight line fit describing the camera's decrease in performance. All the SWP high dispersion beta Lyrae data were corrected using this function.

Wavelengths shortward of 1250 A were not used because of the strongly saturated interstellar Lyman-alpha absorption, which made it difficult to establish reliably the (low) flux levels in that spectral region.

Tables 3 and 4 give, respectively for the SWP and LWP images, IUE flux levels relative to the maximum light at each wavelength, expressed in relative magnitudes. A 70 A bin was used for the 2980 A data in Table 4d as the noise level increases significantly at wavelengths beyond about 3015 A. At any rate, comparison of 70 A and 100 A bins at other wavelengths shows little difference between the two bins except that the 100 A bin light curves look somewhat smoother than the others.

Figures 2 and 3 show respectively the 100 A bin light curves from the IUE spectra.

Figures 1a-1e combine the OAO-A2 and IUE results in one plot. There is an OAO-A2 band centered at 1910 A but at this wavelength the IUE SWP camera becomes noisy for any bin width. For this reason, the OAO-A2 1910 A light curve is paired with the IUE data centered at 1835 A.

The ephemeris used for computing the phases was that of Bahyl, Pikler and Kreiner (1979).

The most remarkable aspect of Figures 1a-1e is that the two light curves agree so well with each other. The consistency of the two light curves, separated typically by more than a decade, is even more remarkable when we note that, over the fifteen day period in 1970, the light curves at shortest wavelengths, especially that at 1430 A, did not quite repeat itself after one orbital period, cf. Figure 1a.

C. Voyager Observations.

The ultraviolet spectrometers (UVS) on board Voyager (Broadfoot et al. 1977) are objective grating instruments sensitive in the 500-1700 A spectral range. The reciprocal dispersion is 9.26 A per detector channel, yielding an effective resolution of about 18 A (about two channels). The Voyager UVS calibration has been discussed by Holberg et al. (1982) and Holberg et al. (1991). During observing periods, the Voyager scan platform is fixed in the normal directions of the target, while the spacecraft limit cycle motions move the field-of-view (FOV) of the spectrometer on and off the target to obtain both source and background signals. In the dispersion direction the transit of a point source through the FOV produces a well-determined Gaussian-like response having an angular half-width of 0.097 degree. In the cross-dispersive direction, the instrument response is approximately rectangular with an approximately 0.86 degree full width.

The majority of the beta Lyrae observations discussed here were obtained with the Voyager 2 UVS during one nearly continuous observing period between 1985 August 3 and 18 (JD 2446281 and 2446296). In addition, two short isolated Voyager 2 observations obtained on 1983 October 5 and on 1984 May 31-June 1 were included in the analysis. For each observing interval, a continuous stream of individual spectra (500-1700 A) of beta Lyr were obtained with an integration time of 3.84 seconds. These individual spectra were combined into 15.36 second averages for logistical reasons. An aspect solution was then performed on the entire data set in order to locate the star within the FOV. The individual spectra obtained at the nominal position of the star in the FOV were accumulated, after removal of sky background, and corrected for all instrumental effects. Throughout the data reduction process we included only the data obtained within

+0.035 degree of the position of beta Lyr within the FOV. During the analysis of the data each successive transit of beta Lyr through the FOV was treated an independent observation. The spectra obtained within a single transit were averaged to improve signal-to-noise ratio. In the case of slow transits of the FOV, the data was subdivided in order to avoid excessive phase smoothing. With UVS data for relatively bright sources such as beta Lyrae, the true photometric error is determined primarily by external factors rather than the photon statistics associated with the measurement. The external errors are, in general, systematic rather than random errors. Specifically, they affect the flux level and not the flux distribution. For the beta Lyr data discussed here these external errors were dominated by the accuracy of the aspect solution. These errors can be evaluated through analysis of stellar transits through the FOV and the spacecraft pointing information. Typically, the effective 1 sigma error bars were found to be 2 to 4 % in the region below 1200 A and 4 to 12 % in the 1200-1700 A region. Table 5 gives the Voyager fluxes for these data.

The Voyager light curves are plotted in Figure 4. The phases were calculated using the light elements by Bahyl et al. (1979). The data at 1430 and 1570 A are basically similar to those from the IUE and the OAO-A2. However, the Voyager light curves at 1085 and 965 A, at which wavelengths we have no observations from either the IUE or the OAO-A2, show no eclipse at all. Over the interval of observation, the 965 A and 1085 A light curves exhibit a slow continuous, non-monotonic, change of intensity with no obvious association with orbital phase (see Figure 4). In addition, there was a significant, "rapid" brightening (a 50% increase in 40 hours), which began near phase 0.55, reached a peak flux near phase 0.7 and continued at this high flux level until the end of the observation near phase 0.8, cf. Figure 5. The brightening can be seen in the longer wavelength Voyager data, but is diluted by the flux of the late-B star. Analysis of this longer wavelength data indicates that throughout this "event" the flux from the late-B star remained constant, other than the variation expected due to changing orbital geometry. This behavior clearly associates the brightening event with the secondary object rather than the late-B star. The brightening occurred only in the continuum; the strong emission line complexes were unaffected. If we take the difference of the outburst and non-outburst spectra, we see an "excess" light that is flat in the far-ultraviolet (912-1200 A) and declines rapidly toward longer wavelengths. As seen in the previous section, the IUE light curves, which were taken over an eight-year period, are consistent and do not show significant deviations; hence, such events probably do not occur frequently. Nevertheless, it is highly desirable to obtain ultraviolet light curves of beta Lyrae continuously over one or more complete orbital periods so as to avoid contaminating the light curves with variations caused by secular events.

No useful data with sufficient signal-to-noise ratio at wavelengths shorter than about 930 A was obtained. The region between 1150 and 1250 A is affected by the interplanetary Lyman-alpha emission and imperfect instrumental scattered light removal, so that Voyager light curve was obtained for the region between 1085 and 1430 A excluding the 1150-1250 A interval.

It should be noted that Figure 1 of Hack et al. (1977) shows both minima to be present but very shallow -- 0.16 mag and 0.24 mag for primary and secondary minimum, respectively -- at wavelength 1035-1060 A.

II. DISCUSSIONS OF THE DATA.

There are two significant results. (A) The secondary minimum, which is clearly shallower than the primary through the mid-ultraviolet wavelengths (longward of 1910 A in the OAO observations), deepens in the far-ultraviolet (shortward of 1910 A) both in the 1970 OAO-2 data and in the IUE data obtained primarily in the 1980s. (B) both the primary minimum and the secondary minimum disappear completely in the shortest wavelength regions of the far-ultraviolet at 1085 and 965 A in the Voyager data obtained mainly in 1985.

A. Deepening of the Secondary Minimum in the Far-Ultraviolet

Clearly, the deepening of the secondary minimum is not a temporary phenomenon unique to the 1970 observations. As was pointed out by Kondo et al. (1971), in the far-ultraviolet we are not observing the light variations caused by the eclipses of two stars of different surface temperatures. If that were the case, the secondary minimum, in which the cooler of the two stars is being eclipsed, would become shallower at shorter wavelengths.

Three other heavily interacting binaries, R Arae and HD

207739 (Kondo, McCluskey and Parsons, 1985) and U Cephei during its dynamic mass flow event in 1974 (Kondo, McCluskey and Wu 1978) and in 1986 (McCluskey, Kondo and Olson 1988) show overwhelming light variations that cannot be understood in terms of the body eclipses of two stars. Milder variations are seen in virtually all active Algol type binaries. The light variations in the three strongly interacting binaries (in the case of U Cep, during the active mass flow events) are possibly caused, at least to a significant extent, by the change of the viewing angle of an optically thick, circumbinary gas. Based on the observed ultraviolet light curves and spectral energy distributions in these binaries over the course of their orbital cycles, this circumbinary gas is always present and highly variable in R Arae and HD 207739, and is present in U Cephei during its active mass flow episodes.

In the case of beta Lyrae, the circumbinary material appears to be fairly stable over a period of some 20 years, although the 1970 light curves indicate that the gas was variable over the 12.9-day orbital period; the light level at the same phase observed 12.9 days later had a lower flux value. Secular variations at the same phase after one or more orbital periods are strongly indicated in the Voyager data (Figure 5). This flux level change was about 15% at 1430 A, 7% at 1550 A and less than 1% at longer wavelengths.

Since the depths of the primary and secondary minima change as a function of the wavelength, the shape and, presumably, the size of the circumbinary gas cloud differs at different wavelengths. This may indicate that the opacity of the gas is wavelength dependent.

Aydin et al. (1988) obtained IUE light curves of beta Lyrae, in a manner similar to that used for this paper, based on spectra obtained from 1978-1980. Many spectra taken with the small aperture were included which increased the uncertainties, since corrections for flux excluded by that aperture are extremely difficult to make. Nonetheless, the conclusions of Aydin et al. (1988) concerning the deepening of secondary minimum in the 1250-1500 A range are in general accord with the results of this paper.

B. Disappearance of the primary and secondary minimum at 1085 and 965 A.

If the optically-thick circumbinary gas assumes a roughly spherical shape completely enveloping the two stars when observed in the shortest far-ultraviolet regions, and if the emission and/or scattering from the circumbinary gas dominates brightness at these wavelengths, light minima can disappear entirely. The energy for keeping the gaseous sphere luminous presumably comes from one or both of the component stars.

The behavior and structure of the far-ultraviolet continuum probably requires the luminous gas to be optically thick. The lack of pronounced aspect variations then implies that the geometry cannot be strongly aspherical. It is not clear, however, that such an optically thick, hot (30,000-70,000 K), luminous (at least 1.5% -- more probably about 5% -- of the brightness of a typical B0 V star at the Voyager wavelengths) gaseous shell can remain relatively stable over a period of two decades, the interval of ultraviolet observation of beta Lyrae.

There is a brightening observed at roughly phase 0.7, which is overlaid on the light curves at 1221, 1365, 1430, 1570 and 1726 A. We interpret this brightening as having been caused by some transient phenomenon such as a giant flare event.

(III) A Broad Brush Picture for beta Lyrae.

Let us attempt to draw a broad-brush picture for beta Lyrae based on these ultraviolet light curves. In the mid-ultraviolet, i.e., longward of about 2000 A, we are basically observing eclipses of two astronomical bodies as we do in visible light. The hotter of the two objects is a late B star, probably B6-B8p. No spectrum has been observed for the cooler object, despite the observed mass function,

$$f(M) = \frac{{M_X}^3}{(M_B + M_X)^2} \sin^3 i = 8.5\ M_\odot$$

which gives it a theoretical minimum mass of 8.5 solar masses. Here, M_B is the mass of the B star and M_X the mass of the spectroscopically undetected object. For any reasonable range of mass for the B component, the mass of the undetected component is 10-15 solar masses. If it is an ordinary star, since it is more massive than the B companion, its spectrum should be detectable and dominate the combined spectrum. The cooler object could be a gas surrounding a very massive object, possibly a collapsed star. At any rate, in visible light and in the mid-ultraviolet, the light curves are those due to the eclipses of two astronomical bodies.

At 1910 A, the circumbinary gas begins to dominate but is still competing with the light from the two stellar or star-like bodies. As a result, both the primary and the secondary minima- are shallower at 1910 A. Indeed, the far-ultraviolet spectrum of beta Lyrae, observed with Copernicus, the Skylab Ultraviolet Experiment and the IUE, is dominated by prominent, multitudinous emission lines (Hack et al. 1975, Kondo et al. 1976).

At shorter wavelengths, e.g., at 1550, 1430 A in the OAO data, at 1570, 1430, 1365 and 1221 A in the IUE data, and at 1570, 1430 and 1365 A in the Voyager observations, the light curves are entirely dominated by radiation from the circumbinary, optically-thick gas cloud. The general shape of the cloud is such that it projects the largest surface area near phases 0.25 and 0.75 and the smallest area near phases 0.0 and 0.5; it might be similar in appearance to an ellipsoid or dumb-bell where the long axis corresponds to the line connecting the two stars. There are two minima of similar amplitudes.

At 1085 and 965 A, the circumbinary cloud still dominates. However, the shape of this cloud seen at these wavelengths is roughly spherical and it engulfs the optically-thick ellipsoidal gas that has been invoked in the foregoing paragraph to account for the light variations at far-ultraviolet wavelengths longer than Lyman-alpha. As a consequence of the roughly spherical shape of this luminous cloud, the light remains approximately constant in this spectral range throughout the orbital period, without any detectable minima.

We have no specific model for the putative circumbinary envelope discussed above. The basic facts are that a very high rate of mass flow occurs in beta Lyrae and that an extensive, complex plasma pervades the system. The behavior of the ultraviolet light curves requires that essentially all of the far-ultraviolet radiation below 1200 A is emitted from uneclipsed regions. An extensive system-enveloping gas would seem more likely than a localized source sufficiently out of the orbital plane to remain uneclipsed but no bet is safe with beta Lyrae. Future investigators must address the scattering and emitting properties of the beta Lyrae plasma.

(IV) Closing Remarks

Thus far, four interacting binaries, beta Lyrae, R Arae, HD 207739, and U Cephei (during its active phase), have been found to be shrouded in optically thick circumbinary envelopes. There are also many other active binaries that exhibit evidence for the presence of optically thick gas. There may be more undetected binary systems in this phase of evolution. Because of the temperature of this circumbinary plasma, the ultraviolet spectral region is probably optimally suited for its detection.

Are these binary systems in the so-called dynamic phase of mass flow, which is assumed to last only thousands of years? If one defines the phase of dynamic mass flow as that in which one of the components has evolved to fill its critical Roche -- or

Jacobian -- equipotential surface and is overflowing that surface on a Kelvin-Helmholtz time scale, our answer is uncertain since we are at the moment unable to determine the physical parameters of these binaries with sufficient accuracy because of the presence of the optically thick circumbinary cloud. In the case of beta Lyrae, the mass ratio is rather extreme for the dynamic mass flow model to apply in a conventional sense.

Whatever this phase turns out to be in the evolutionary course of binaries, it is probably a relatively short lived one, since few systems have been observed at this evolutionary stage. Nevertheless, it is likely a profoundly important stage since a large quantity of circumbinary matter is involved and also, in all four cases, a considerable amount of matter is being lost from the binary system (Hack et al. 1977, Kondo, McCluskey and Stencel 1979, McCluskey and Kondo 1983, Parsons, Holm and Kondo 1983, McCluskey, Kondo and Olson 1988).

Acknowledgement

It is a pleasure to acknowledge the competent assistance of Babar Ali in Voyager data reduction. We would like to dedicate this paper to the memory of our late colleague Ted Houck and to John Goodricke (1765-1787), who first suggested the binary nature of the light variations in beta Lyrae from his own careful observations.

References

Aydin, C., Brandi, E., Engin, S., Ferrer, O.E., Hack, M., Sahade, J., Solivella, G. and Yilmaz, N. 1988, Astron.Ap., 193, 202.

Broadfoot, A.L. et al. 1977, Space Sci. Rev., 21, 183.

Hack, M., Hutchings, J.B., Kondo, Y., McCluskey, G.E., Plavec, M. and Polidan, R.S. 1975, Ap.J., 198, 453.

Hack, M., Hutchings, J.B., Kondo, Y., and McCluskey, G.E. 1977, Ap.J.Suppl., 34, 565.

Holberg, J. B., Forrester, W.T., Shemansky, E.E. and Barry, D.C. 1982, Ap.J., 257, 656.

Holberg, J.B., Ali, B., Carone, T.E. and Polidan, R.S. 1991, Ap.J., 375, 716.

Kondo, Y., Hack, M., Hutchings, J.B., McCluskey, G.E., Plavec, M. and Polidan 1976, Ap. & Space Sci., 38, 353.

Kondo, Y., McCluskey, G.E. and Houck, T.E. 1971, Proc. of IAU Colloq. No. 15, 308.

Kondo, Y., McCluskey, G.E. and Houck, T.E. 1972, Proc. of OAO Symposium, 485.

Kondo, Y., McCluskey, G.E. and Eaton, J.A. 1976, Ap. & Space Sci., 41, 121.

Kondo, Y., McCluskey, G.E. and Parsons, S.B. 1985, Ap.J., 295, 580.

Kondo, Y., McCluskey, G.E. and Stencel, R.E. 1979, Ap.J., 233, 906.

Kondo, Y., McCluskey, G.E. and Wu, C.-C. 1978, Ap.J., 222, 635.

McCluskey, G.E., Kondo, Y. and Olson, E.C. 1988, Ap.J., 332, 1019.

Parsons, S.B., Holm, A.V. and Kondo, Y. 1983, Ap.J. (Lett.), 264, L19.

Wood, D.B., and Forbes, J.E. 1963, Ap.J., 68, 257.

Figure Legends

Figures 1a-1e. OAO-A2 and IUE Light Curves, plotted together for comparison, at 1430 vs. 1430, 1550 vs. 1570, 1910 vs. 1835, 2460 vs. 2470, and 2980 vs. 2980 A, respectively. Boxes represent OAO, and + and x signs indicate IUE data. OAO and IUE wavelengths are not perfectly matched at some wavelengths for the reasons explained in the text. As the OAO-A2 observations were made over a 15-day-plus period, there is an overlap at phase 0.75-1.0.

Figures 2a-2d. IUE SWP Light Curves at 1250, 1365, 1726 and 1835 A, respectively.

Figures 3a-3b. IUE LWP Light Curves at 2180 and 2720 A, respectively.

Figures 4a-4d. Voyager Light Curves at 965, 1085, 1430 and 1570 A, respectively.

Figure 5. Voyager data at 965 A, 1985 August 3-18, showing the brightening in time sequence rather than as a function of phase.

List of Tables

Addresses

Yoji Kondo, Code 684, Goddard Space Flight Center, Greenbelt, MD 20771

George E. McCluskey, Division of Astronomy, Department of Mathematics, Lehigh University, Bethlehem, PA 18018

Jeffrey M.S. Silvis, Department of Physics, The Catholic University of America, Washington, DC 20064

Ronald S. Polidan, Code 681, Goddard Space Flight Center, Greenbelt, MD 20771

Carolina P.S. McCluskey, Department of Computer Science, The Pennsylvania State University, Allentown Campus, Foglesville, PA 18051

Joel A. Eaton, Tennessee State University, Center of Excellence in Information Systems, 330 10th Avenue North, Ste. 265, Nashville, TN 37203-3401

Figure 1a

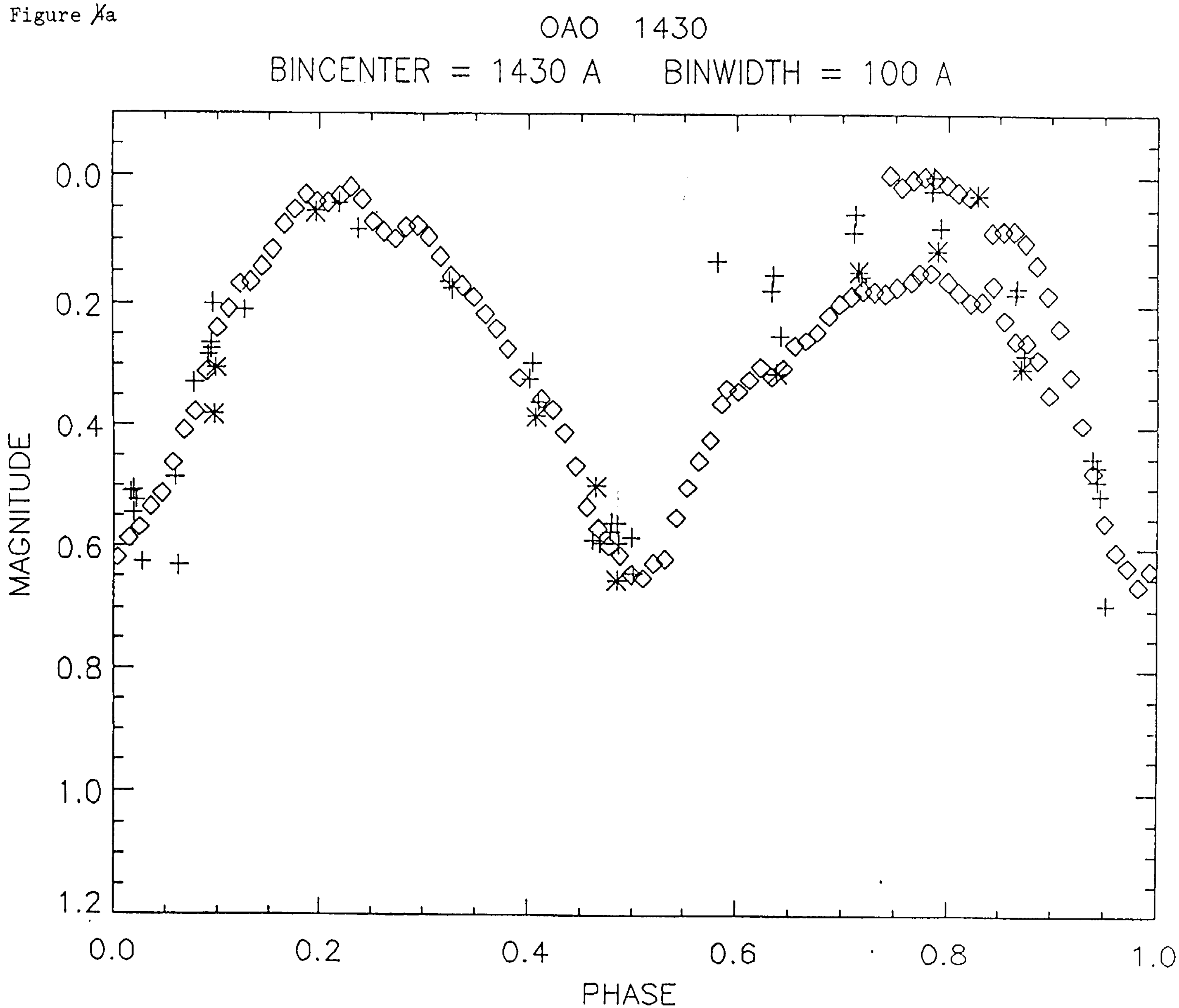
OAO 1430
BINCENTER = 1430 A BINWIDTH = 100 A
MAGNITUDE
0.0
0.2
0.4
0.6
0.8
1.0
1.2
0.0
0.2
0.4
0.6
0.8
1.0
PHASE

Figure 1b

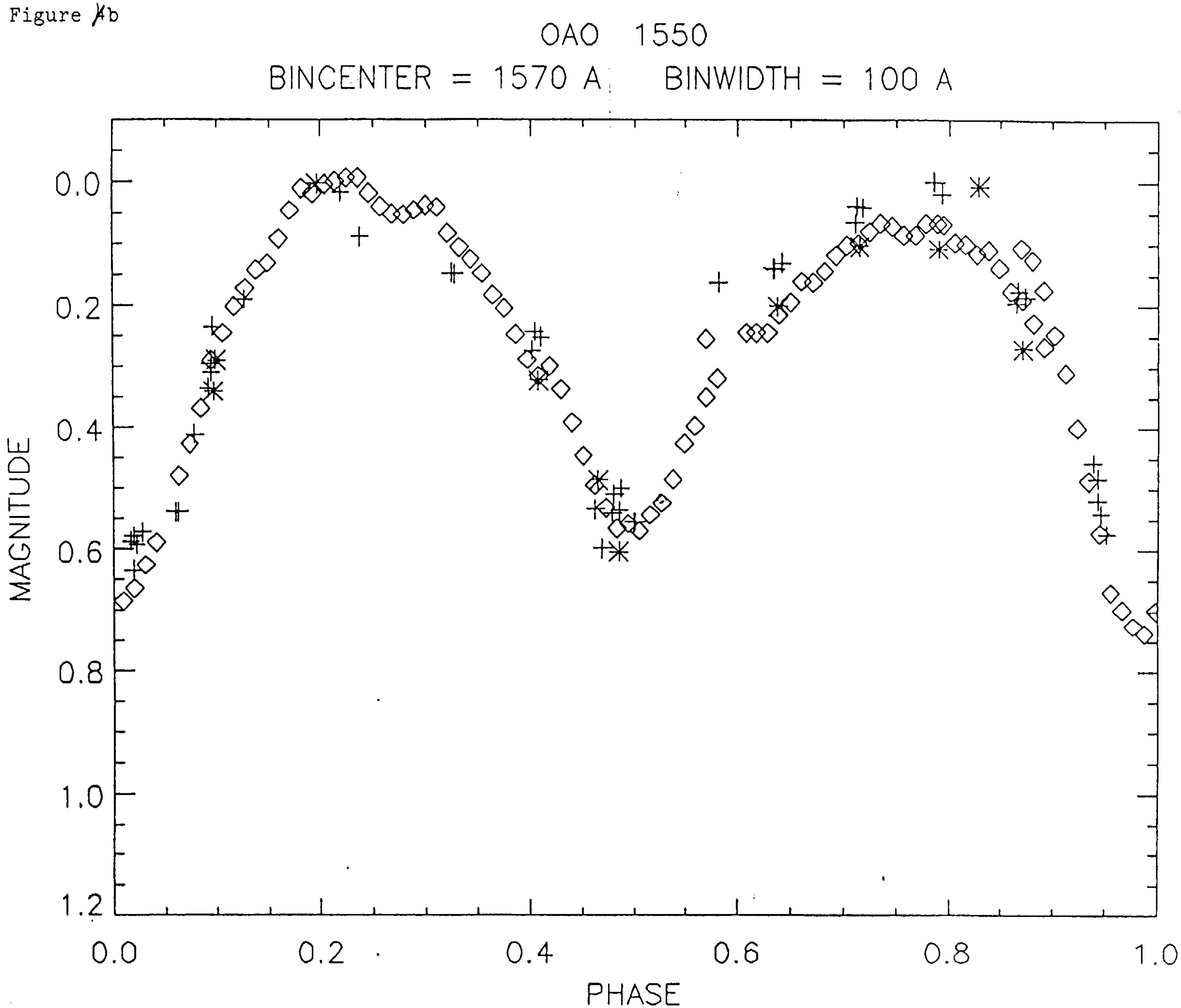
OAO 1550
BINCENTER = 1570 A BINWIDTH = 100 A
MAGNITUDE
0.0
0.2
0.4
0.6
0.8
1.0
1.2
0.0
0.2
0.4
0.6
0.8
1.0
PHASE

Figure 1c

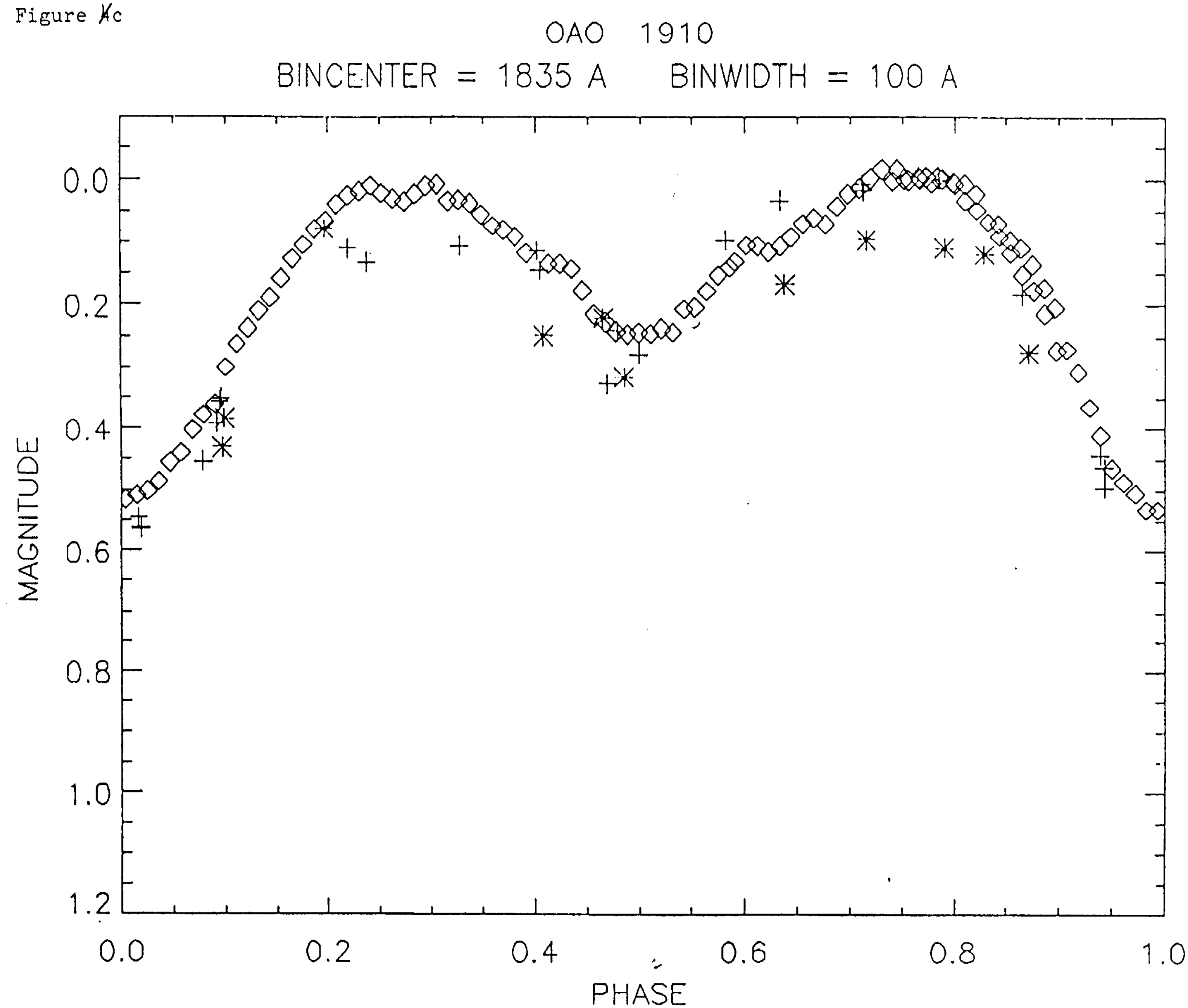

OAO 1910
BINCENTER = 1835 A BINWIDTH = 100 A
MAGNITUDE
PHASE
0.0
0.2
0.4
0.6
0.8
1.0
1.2

Figure 1d

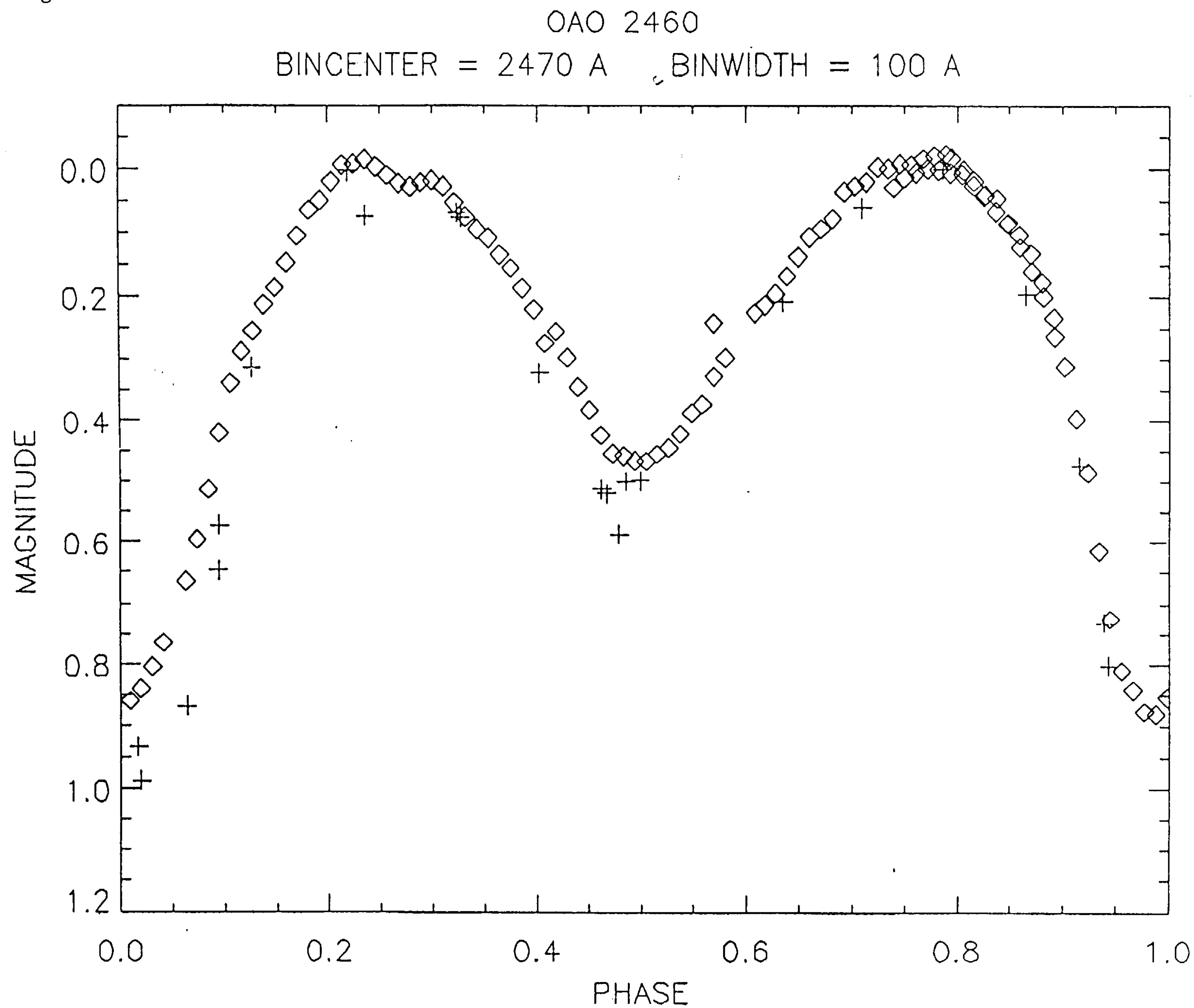
OAO 2460
BINCENTER = 2470 A BINWIDTH = 100 A
MAGNITUDE
0.0
0.2
0.4
0.6
0.8
1.0
1.2
0.0
0.2
0.4
0.6
0.8
1.0
PHASE

Figure 1e

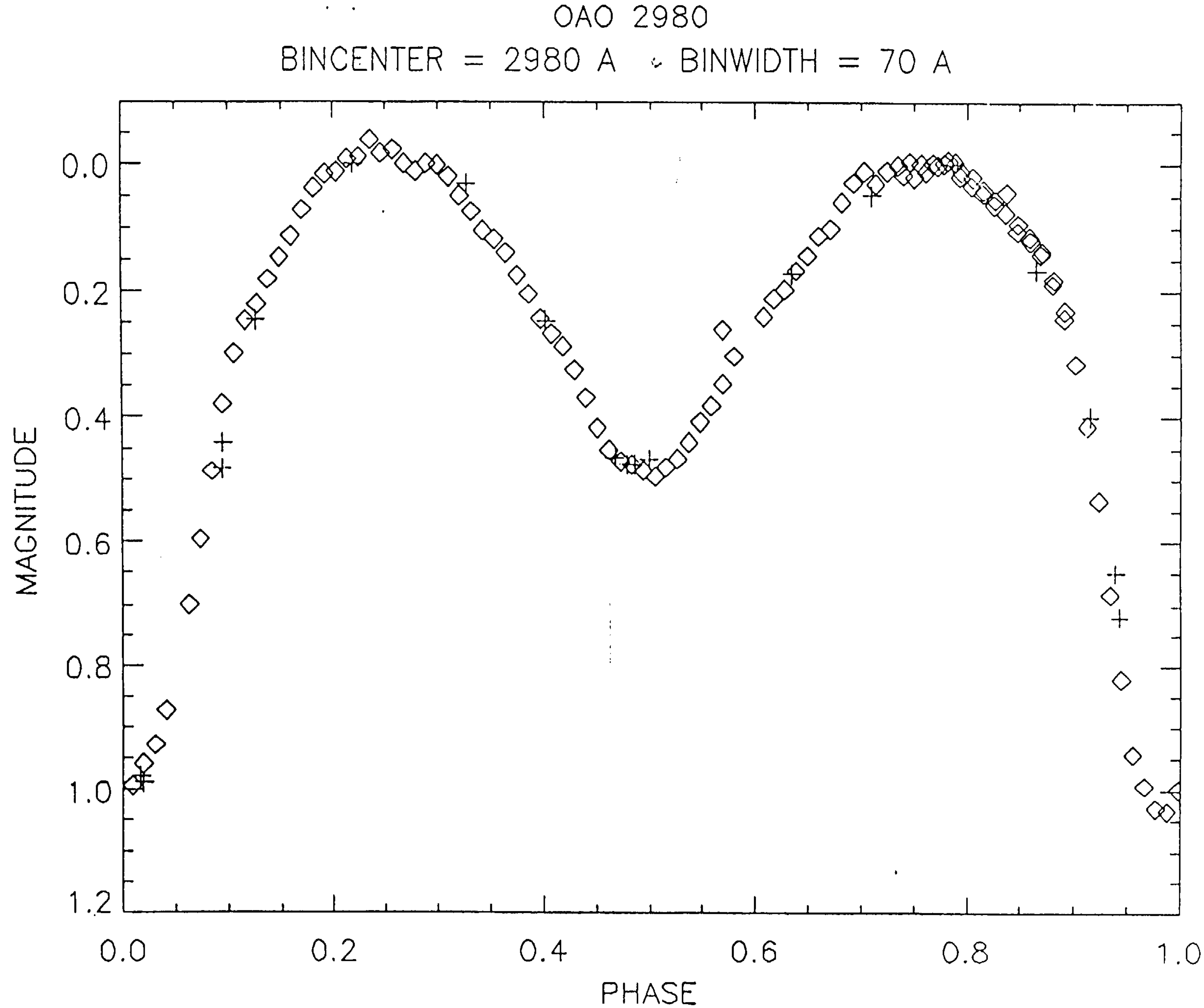
OAO 2980
BINCENTER = 2980 A , BINWIDTH = 70 A
MAGNITUDE
0.0
0.2
0.4
0.6
0.8
1.0
1.2
PHASE
0.0
0.2
0.4
0.6
0.8
1.0

Figure 2b

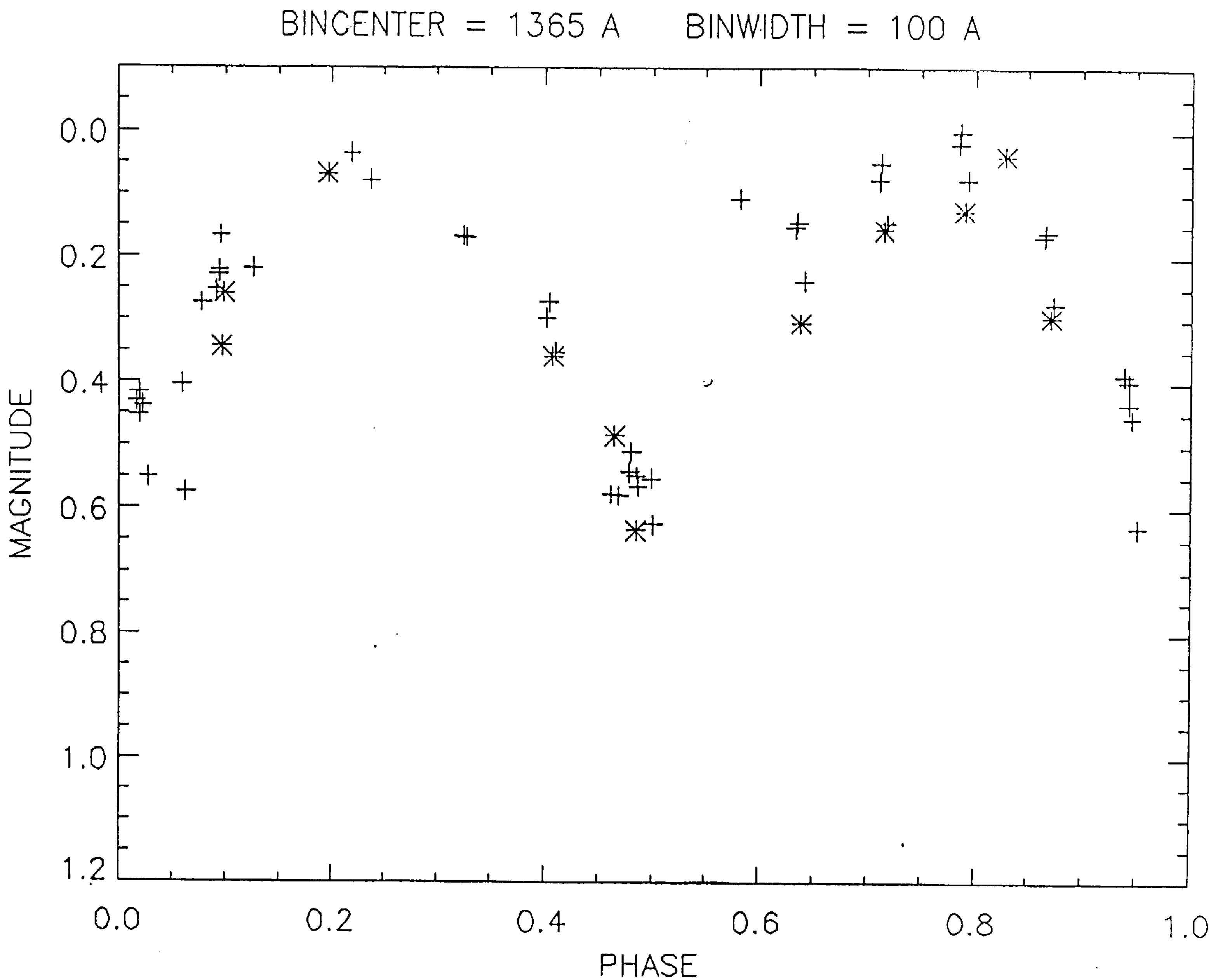
BINCENTER = 1365 A BINWIDTH = 100 A
MAGNITUDE
0.0
0.2
0.4
0.6
0.8
1.0
1.2
0.0
0.2
0.4
0.6
0.8
1.0
PHASE

Figure 2c

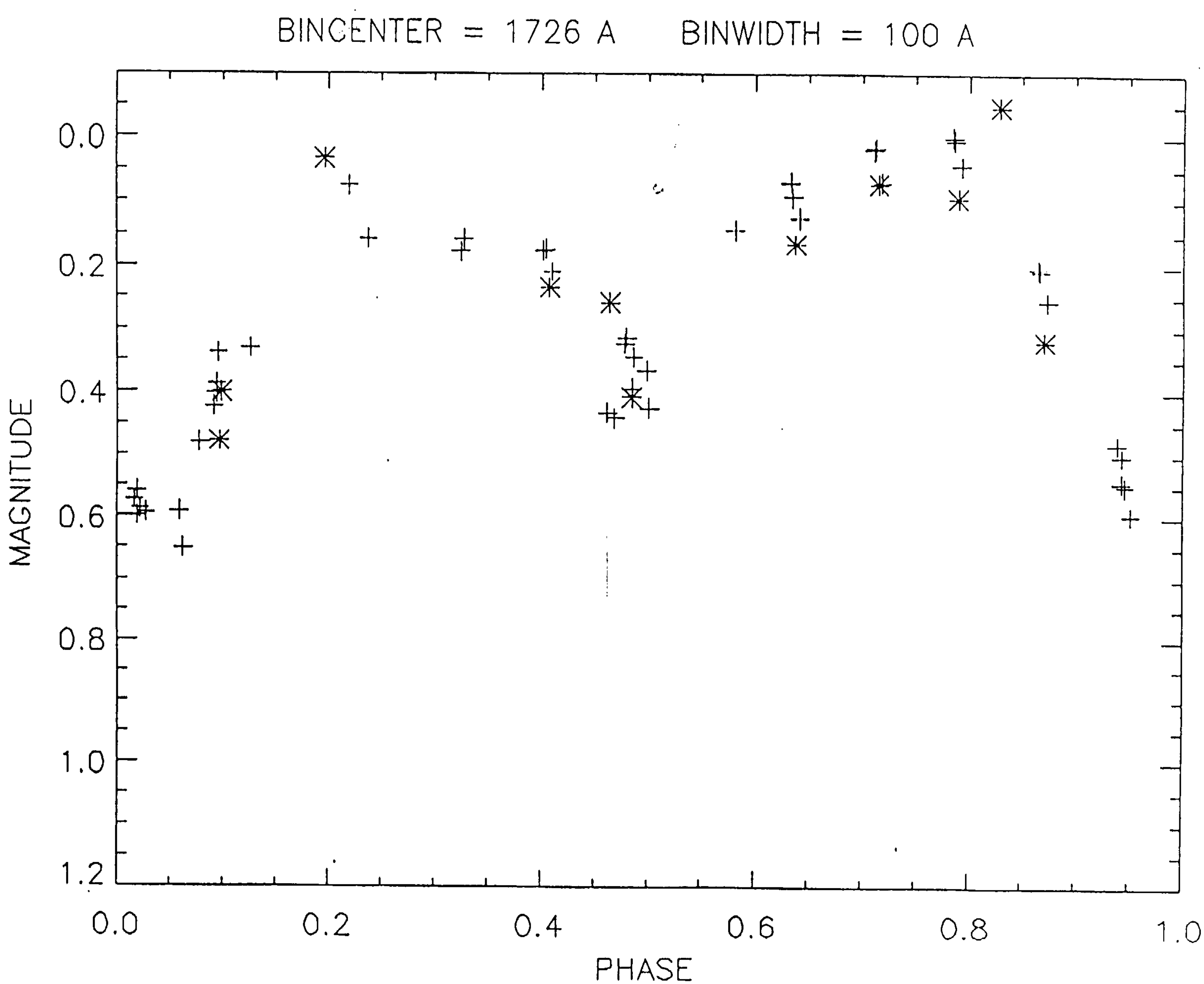
BINCENTER = 1726 A BINWIDTH = 100 A
MAGNITUDE
PHASE
0.0
0.2
0.4
0.6
0.8
1.0
1.2

Figure 2d

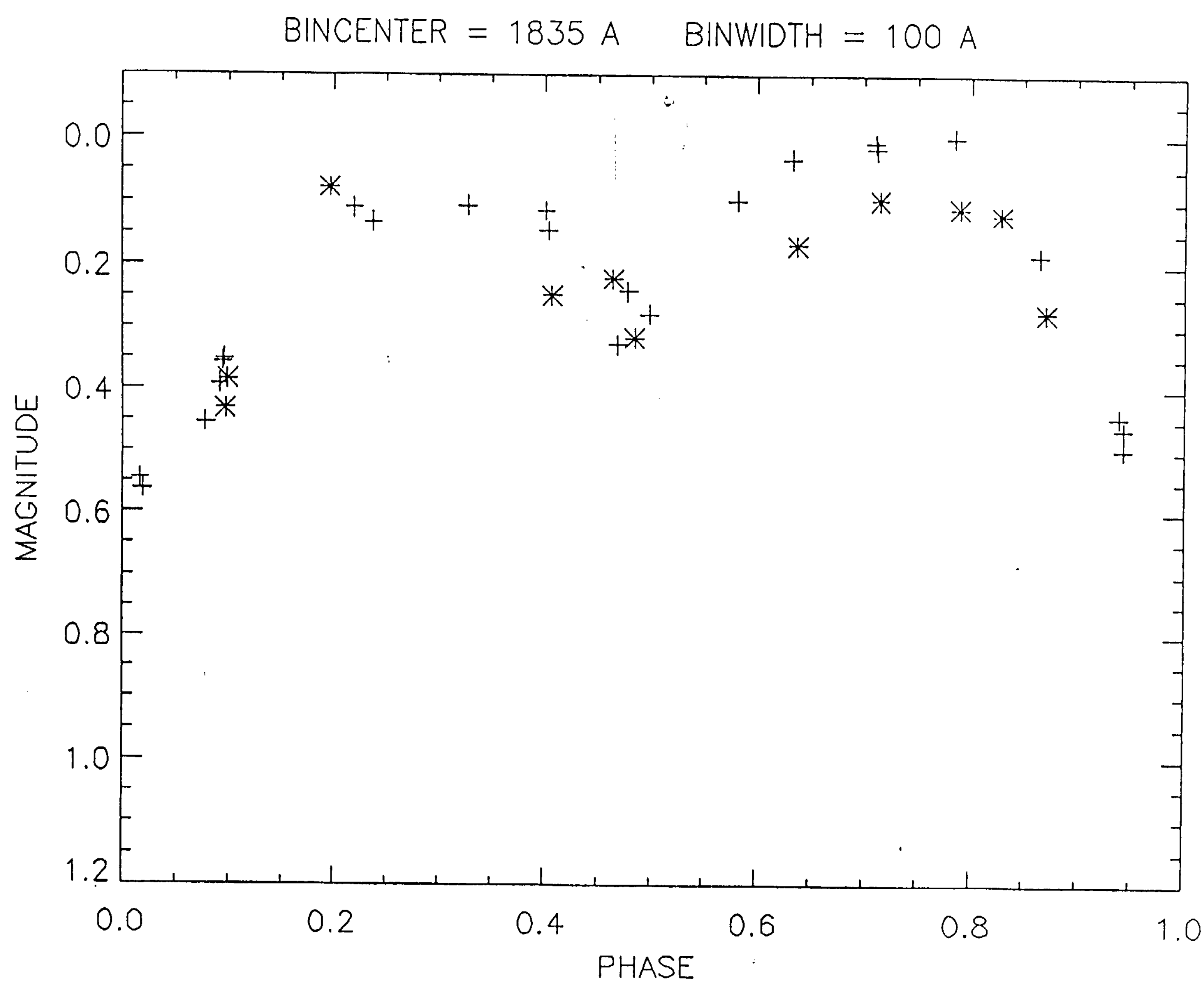
BINCENTER = 1835 A BINWIDTH = 100 A
MAGNITUDE
0.0
0.2
0.4
0.6
0.8
1.0
1.2
0.0
0.2
0.4
0.6
0.8
1.0
PHASE

Figure 3a

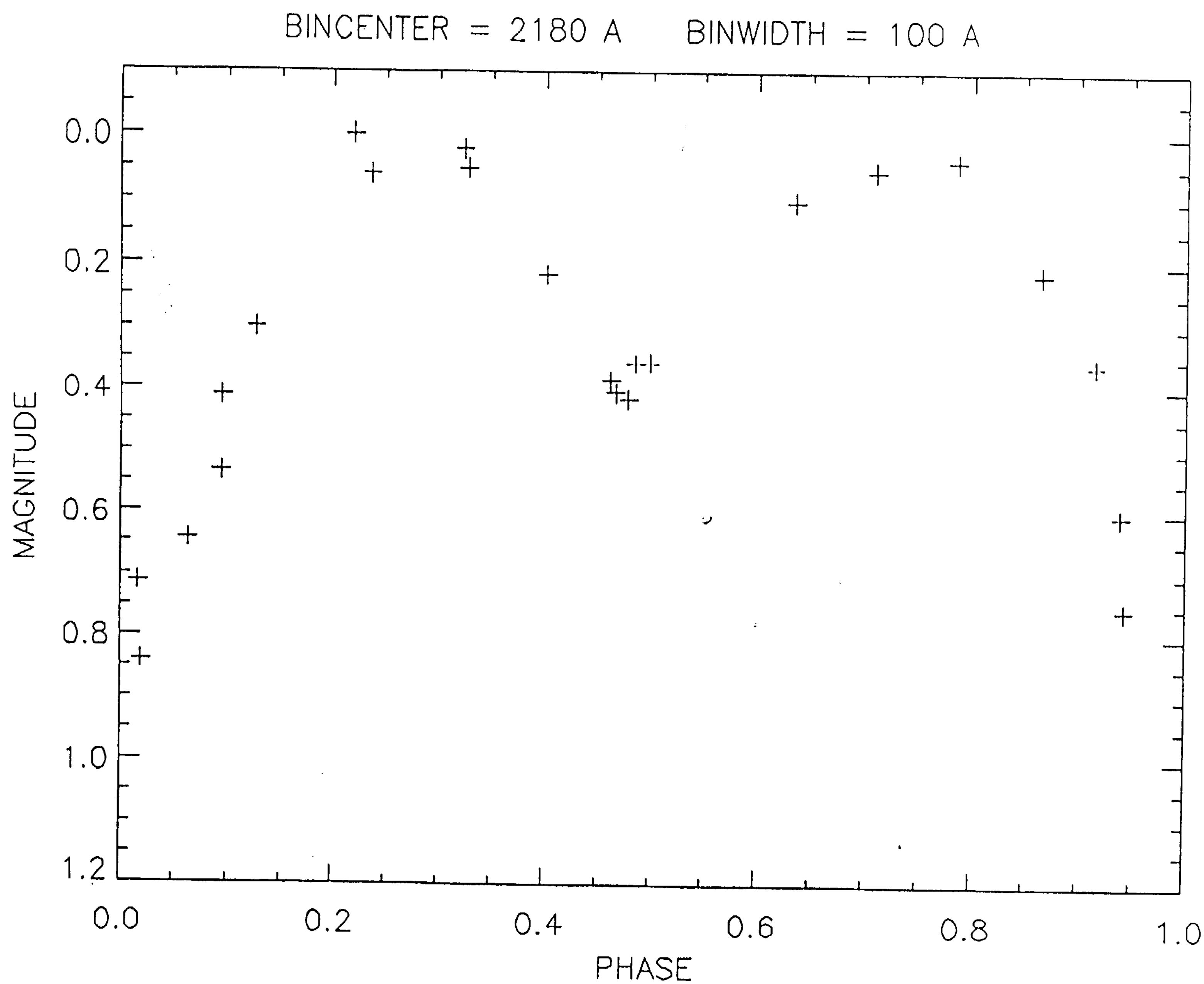

BINCENTER = 2180 A BINWIDTH = 100 A
MAGNITUDE
0.0
0.2
0.4
0.6
0.8
1.0
1.2
0.0
0.2
0.4
0.6
0.8
1.0
PHASE

Figure 3b

BINCENTER = 2720 A   BINWIDTH = 100 A

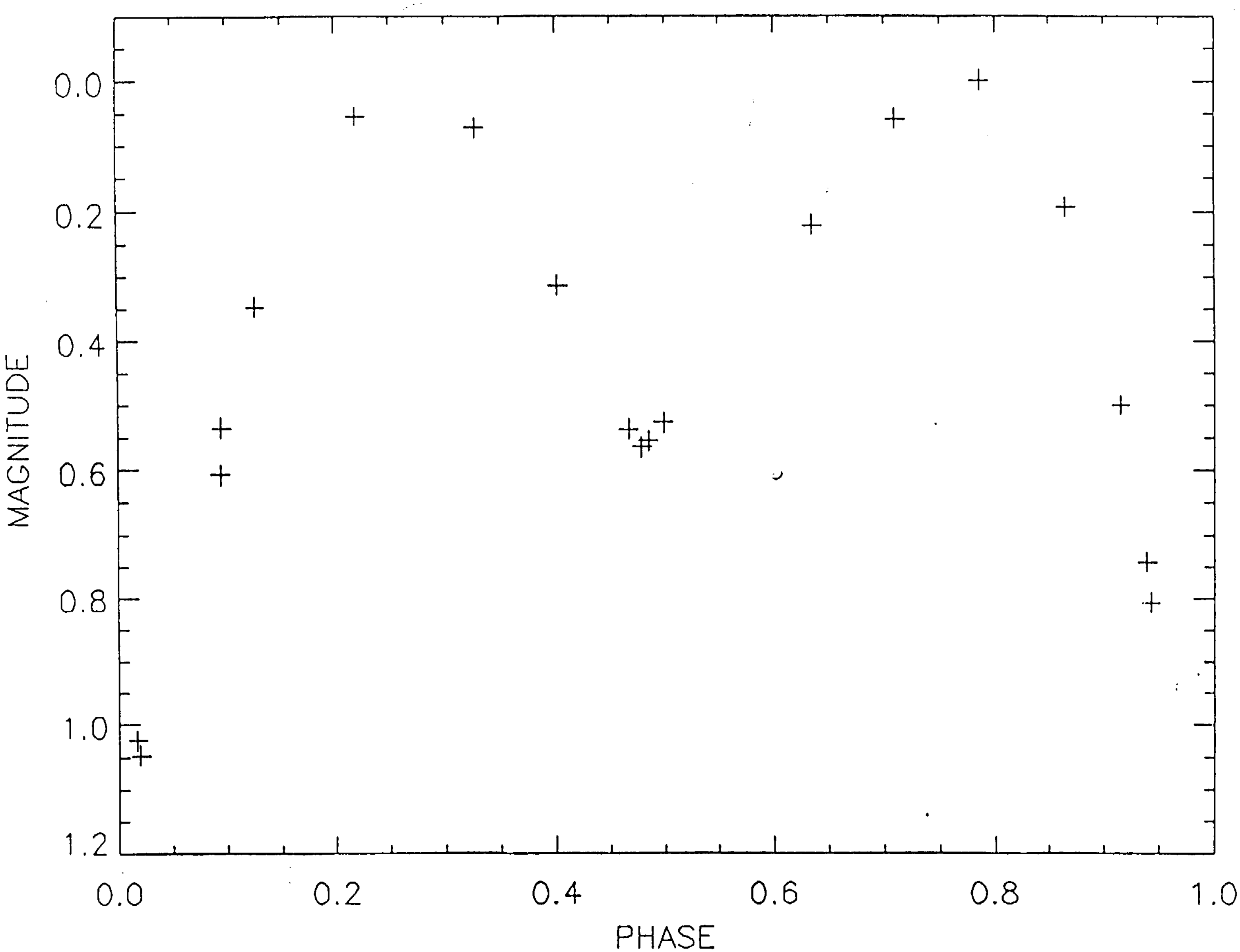

Figure 4a

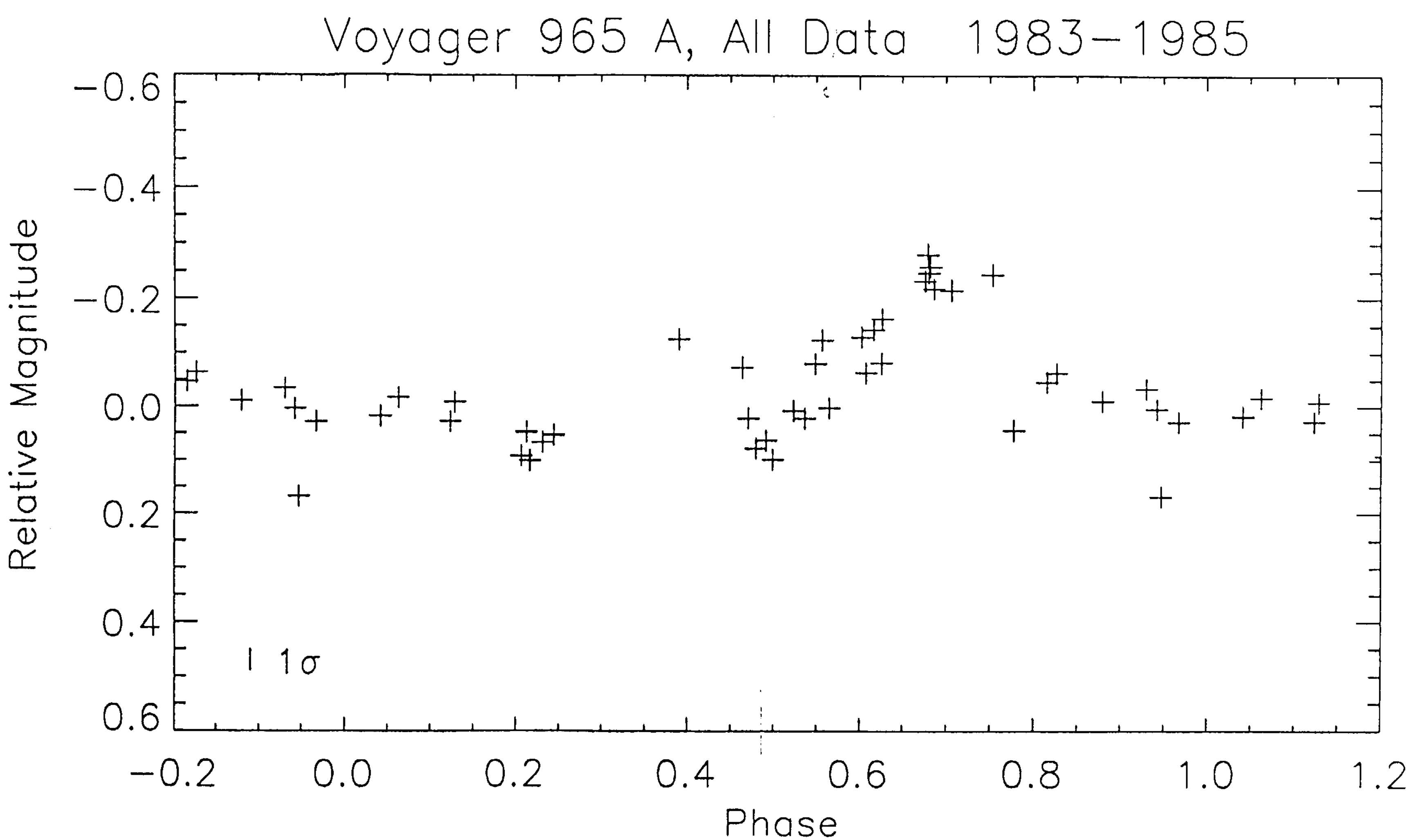
Voyager 965 A, All Data 1983–1985
Relative Magnitude
−0.6
−0.4
−0.2
0.0
0.2
0.4
0.6
1σ
−0.2
0.0
0.2
0.4
0.6
0.8
1.0
1.2
Phase

Figure 4b

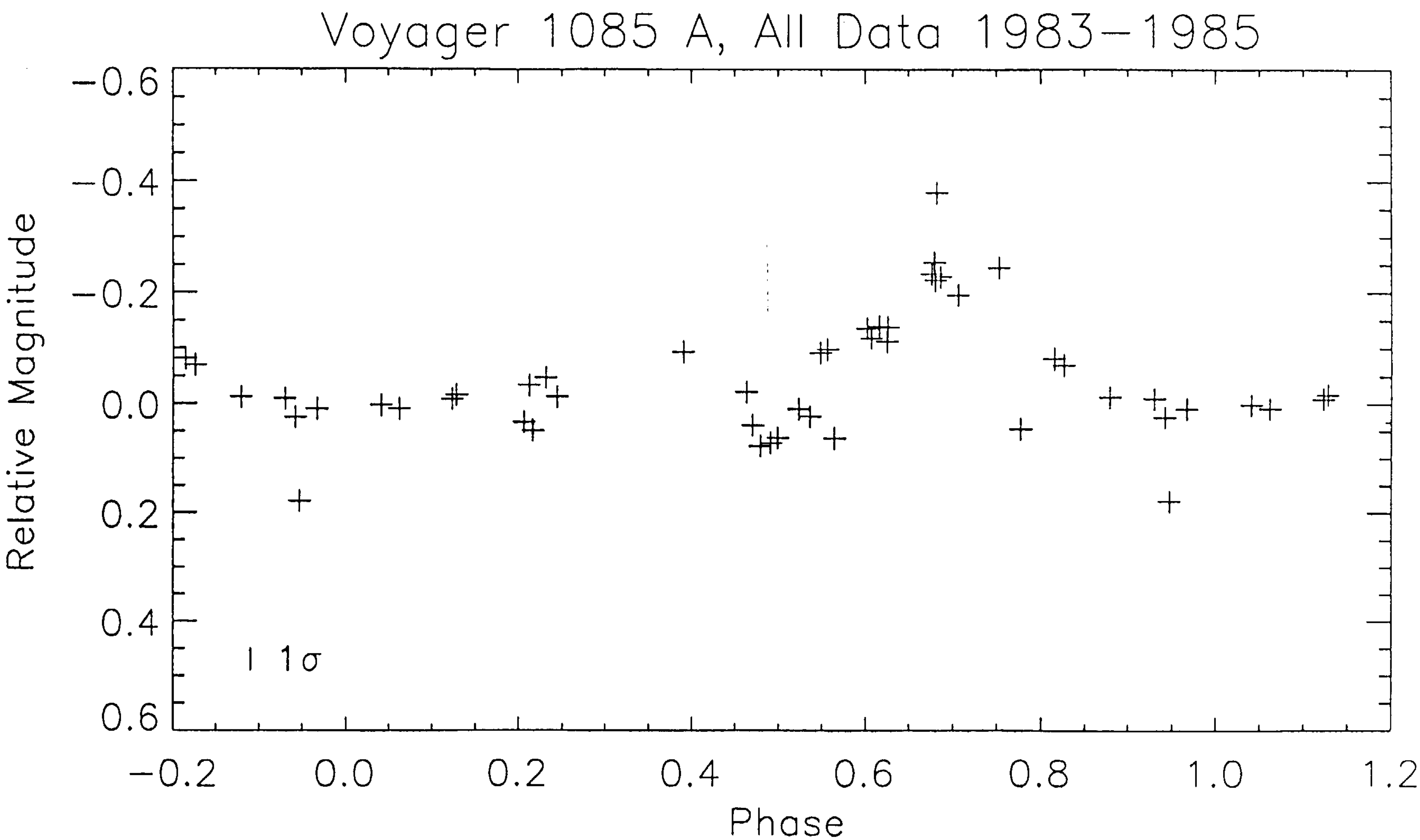

Voyager 1085 A, All Data 1983–1985
Relative Magnitude
−0.6
−0.4
−0.2
0.0
0.2
0.4
0.6
1σ
−0.2
0.0
0.2
0.4
0.6
0.8
1.0
1.2
Phase

Figure 4c

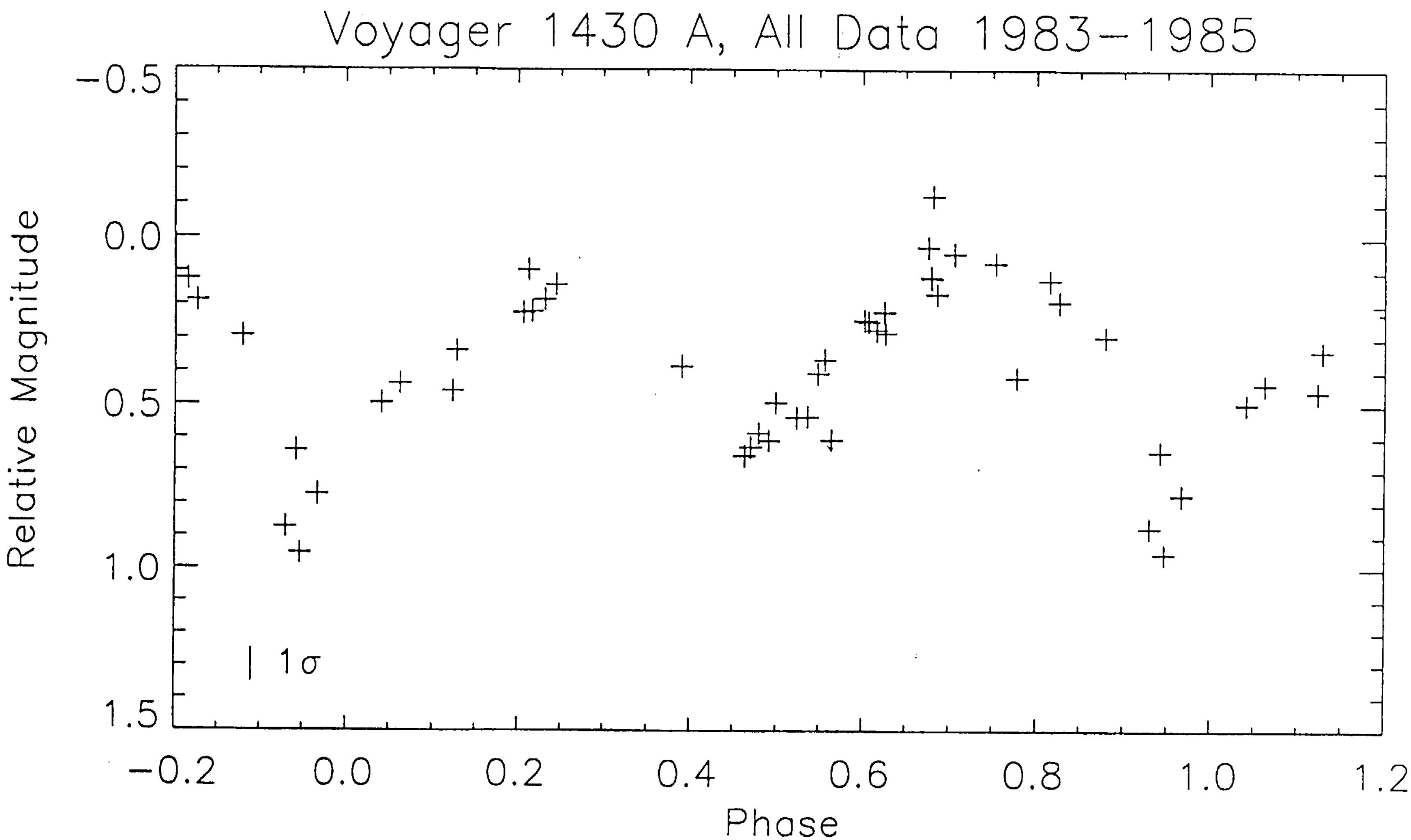

Voyager 1430 A, All Data 1983–1985
Relative Magnitude
Phase
−0.5
0.0
0.5
1.0
1.5
−0.2
0.0
0.2
0.4
0.6
0.8
1.0
1.2
1σ

Figure 4d

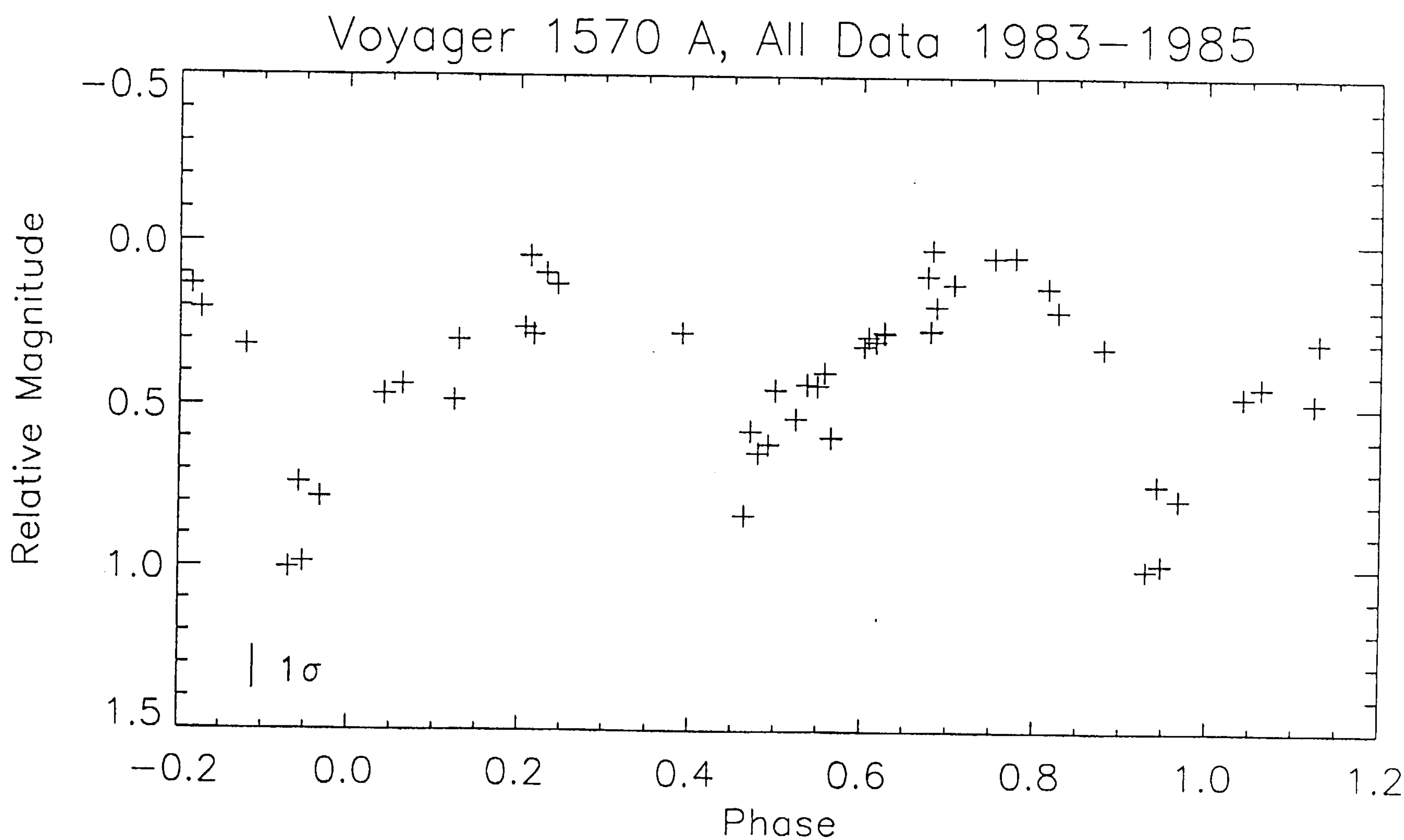
Voyager 1570 A, All Data 1983–1985
Relative Magnitude
Phase
−0.5
0.0
0.5
1.0
1.5
−0.2
0.0
0.2
0.4
0.6
0.8
1.0
1.2
1σ

Figure 5

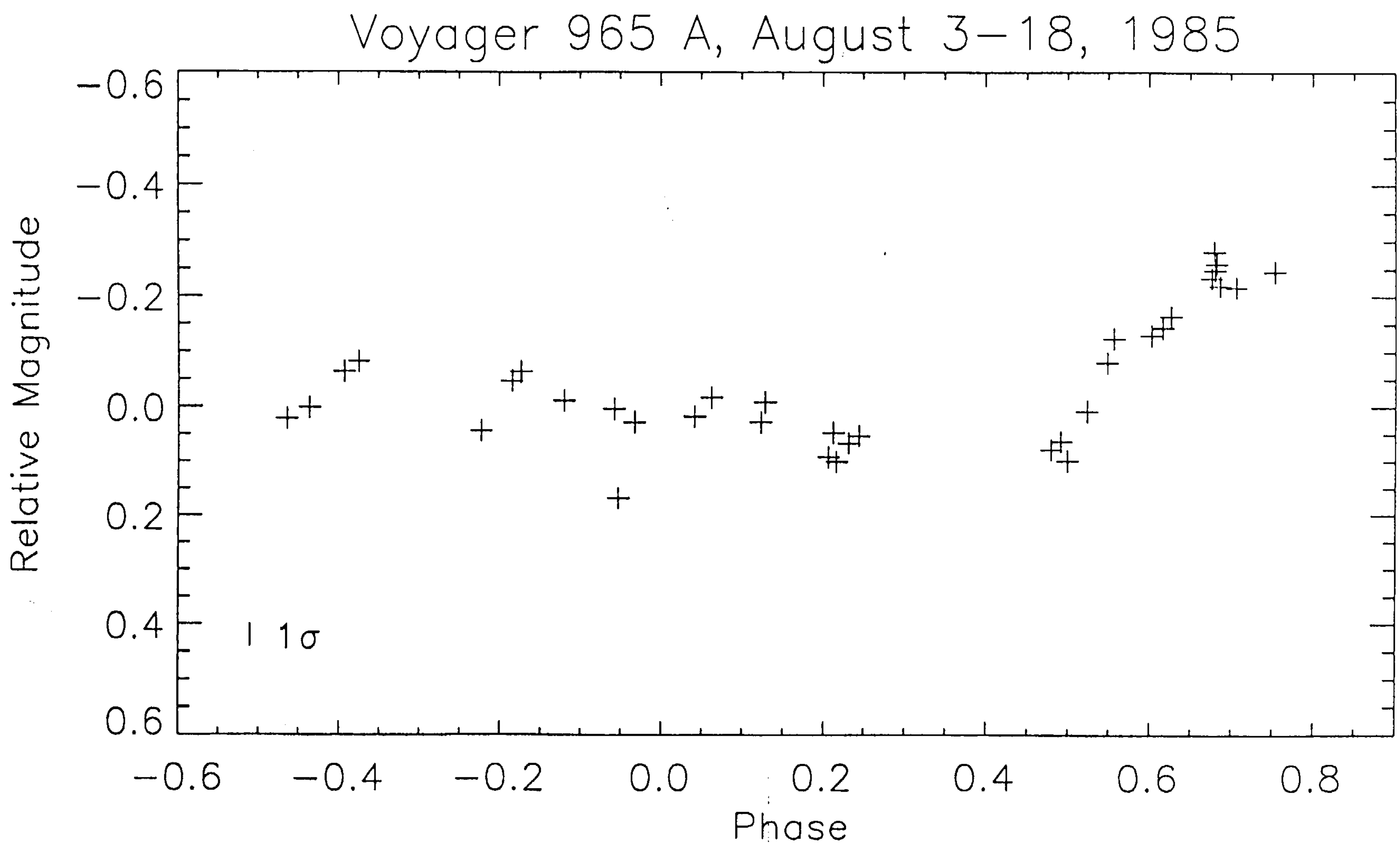
Voyager 965 A, August 3–18, 1985
Relative Magnitude
−0.6
−0.4
−0.2
0.0
0.2
0.4
0.6
1σ
−0.6
−0.4
−0.2
0.0
0.2
0.4
0.6
0.8
Phase

List of Tables

TABLE I

OAO-2 photometry of β Lyrae

Observations at 2980 Å, 2460 Å, and 1550 Å

JD⊙ 2 440 000+	Phase	m_λ 2980	2460	1550	JD⊙ 2 440 000+	Phase	m_λ 2980	2460	1550
889.4909	0.7402	0.017	0.029	0.012	897.1472	0.3322	0.074	0.076	0.106
889.6301	0.7509	0.020	0.013	0.005	897.2865	0.3429	0.104	0.095	0.125
889.7692	0.7617	0.012	0.006	0.007	897.4257	0.3537	0.118	0.108	0.148
889.9085	0.7724	0.002	0.000	−0.005	897.5650	0.3645	0.139	0.134	0.183
890.0477	0.7832	−0.005	0.001	0.002	897.7042	0.3752	0.175	0.155	0.204
890.1868	0.7940	0.019	0.006	−0.001	897.8433	0.3860	0.205	0.187	0.247
890.3260	0.8047	0.034	0.009	0.014	897.9826	0.3968	0.244	0.220	0.288
890.4653	0.8155	0.046	0.026	0.031	898.1218	0.4075	0.267	0.274	0.315
890.6045	0.8263	0.063	0.043	0.037	898.2611	0.4183	0.287	0.255	0.298
890.7436	0.8370	0.076	0.066	0.068	898.4004	0.4291	0.324	0.297	0.336
890.8828	0.8478	0.105	0.086	0.087	898.5396	0.4398	0.369	0.344	0.391
890.8836	0.8478	0.105	0.086	0.089	898.6788	0.4506	0.417	0.382	0.445
891.0221	0.8586	0.114	0.103	0.081	898.8181	0.4614	0.451	0.423	0.494
891.1612	0.8693	0.141	0.132	0.106	898.9573	0.4721	0.469	0.453	0.531
891.3004	0.8801	0.188	0.177	0.125	899.0968	0.4829	0.475	0.457	0.564
891.4397	0.8908	0.242	0.233	0.173	899.2360	0.4937	0.484	0.465	0.556
891.5787	0.9016	0.314	0.311	0.246	899.3753	0.5045	0.494	0.466	0.568
891.7179	0.9124	0.413	0.396	0.309	899.5145	0.5152	0.479	0.454	0.542
891.8572	0.9231	0.532	0.484	0.399	899.6538	0.5260	0.465	0.444	0.523
891.9965	0.9339	0.682	0.614	0.486	899.7930	0.5368	0.439	0.421	0.484
892.1357	0.9447	0.821	0.725	0.571	899.9323	0.5475	0.407	0.387	0.425
892.2748	0.9554	0.943	0.810	0.669	900.0716	0.5583	0.382	0.373	0.396
892.4141	0.9662	0.993	0.842	0.698	900.2110	0.5691	0.347	0.327	0.349
892.5531	0.9769	1.029	0.877	0.725	900.3501	0.5798	0.302	0.297	0.318
892.6923	0.9877	1.034	0.881	0.737	900.5590	0.5690	0.260	0.241	0.254
892.8316	0.9985	0.999	0.854	0.699	900.6983	0.6068	0.240	0.225	0.244
892.9708	0.0092	0.994	0.860	0.685	900.8334	0.6172	0.211	0.213	0.244
893.1099	0.0200	0.959	0.840	0.664	900.9723	0.6279	0.197	0.195	0.244
893.2492	0.0308	0.929	0.805	0.625	901.1112	0.6387	0.167	0.167	0.214
893.3885	0.0415	0.873	0.765	0.588	901.2521	0.6496	0.143	0.137	0.194
893.6667	0.0630	0.699	0.665	0.479	901.3910	0.6603	0.112	0.106	0.160
893.8060	0.0738	0.595	0.596	0.426	901.5306	0.6711	0.101	0.093	0.161
893.9452	0.0846	0.485	0.513	0.368	901.6702	0.6819	0.059	0.077	0.143
894.0845	0.0954	0.380	0.420	0.290	901.8091	0.6926	0.029	0.036	0.118
894.2237	0.1061	0.298	0.339	0.245	901.9493	0.7035	0.012	0.027	0.102
894.3628	0.1169	0.246	0.287	0.202	902.0880	0.7142	0.031	0.020	0.099
894.5020	0.1276	0.221	0.255	0.172	902.2269	0.7250	0.011	−0.002	0.080
894.6413	0.1384	0.181	0.213	0.142	902.3658	0.7357	0.002	−0.000	0.066
894.7805	0.1492	0.146	0.186	0.131	902.5047	0.7464	−0.004	−0.007	0.071
894.9196	0.1599	0.113	0.147	0.092	902.6436	0.7572	−0.000	−0.006	0.085
895.0588	0.1707	0.072	0.105	0.046	902.7832	0.7680	−0.001	−0.016	0.085
895.1981	0.1815	0.038	0.065	0.011	902.9228	0.7788	−0.001	−0.020	0.066
895.3373	0.1922	0.017	0.050	0.019	903.0617	0.7895	−0.002	−0.022	0.066
895.4764	0.2030	0.013	−0.020	0.005	903.1318	0.7949	0.012	−0.017	0.068
895.6158	0.2138	−0.007	0.006	0.000	903.2714	0.8057	0.020	0.002	0.097
895.7549	0.2245	−0.010	−0.007	−0.006	903.4103	0.8165	0.040	0.019	0.100
895.8941	0.2353	−0.038	−0.014	−0.006	903.5499	0.8272	0.055	0.040	0.115
896.0334	0.2460	−0.017	−0.003	0.019	903.6881	0.8379	0.044	0.046	0.109
896.1727	0.2568	−0.022	0.010	0.040	903.8277	0.8487	0.093	0.084	0.138
896.3119	0.2676	0.000	0.023	0.052	903.9679	0.8596	0.120	0.122	0.176
896.4510	0.2783	0.012	0.028	0.053	904.1068	0.8703	0.137	0.160	0.190
896.5911	0.2892	−0.000	0.022	0.046	904.2457	0.8810	0.181	0.199	0.227
896.7295	0.2999	0.002	0.019	0.038	904.3838	0.8917	0.230	0.263	0.266
896.8687	0.3106	0.020	0.028	0.041					

Observations at 3320 Å, 1910 Å, and 1430 Å

JD⊙ 2 440 000+	Phase	m_λ 3320	1910	1430	JD⊙ 2 440 000+	Phase	m_λ 3320	1910	1430
889.5604	0.7455	0.001	−0.014	−0.002	897.2170	0.3376	0.056	0.038	0.171
889.6997	0.7563	0.003	0.001	0.016	897.3560	0.3483	0.073	0.056	0.188
889.8389	0.7671	0.003	0.000	0.005	897.4953	0.3591	0.097	0.074	0.215
889.9782	0.7778	0.000	0.005	0.000	897.6345	0.3698	0.132	0.081	0.239
890.1173	0.7886	0.010	−0.001	0.002	897.7738	0.3806	0.157	0.092	0.272
890.2565	0.7994	0.011	0.004	0.011	897.9130	0.3914	0.192	0.118	0.319
890.3956	0.8101	0.027	0.007	0.024	898.1916	0.4129	0.252	0.135	0.354
890.5348	0.8209	0.034	0.023	0.031	898.3308	0.4237	0.274	0.135	0.372
890.8133	0.8424	0.063	0.070	0.085	898.4701	0.4345	0.324	0.143	0.410
890.9524	0.8532	0.077	0.097	0.082	898.6093	0.4452	0.361	0.178	0.464
890.9531	0.8532	0.071	0.097	0.084	898.7485	0.4560	0.407	0.215	0.532
891.0916	0.8639	0.091	0.109	0.083	898.8878	0.4668	0.425	0.227	0.567
891.2309	0.8747	0.121	0.135	0.101	899.0270	0.4775	0.443	0.242	0.596
891.3700	0.8855	0.172	0.173	0.135	899.1663	0.4883	0.460	0.246	0.612
891.5092	0.8962	0.224	0.204	0.182	899.3056	0.4991	0.474	0.244	0.642
891.6484	0.9070	0.314	0.269	0.235	899.4448	0.5098	0.460	0.245	0.649
891.7877	0.9178	0.423	0.306	0.314	899.5840	0.5206	0.452	0.237	0.624
891.9269	0.9285	0.569	0.364	0.395	899.7233	0.5314	0.464	0.243	0.617
892.0660	0.9393	0.732	0.411	0.472	899.8628	0.5421	0.414	0.207	0.549
892.2053	0.9500	0.878	0.463	0.555	900.0020	0.5529	0.374	0.204	0.499
892.3444	0.9608	0.959	0.485	0.603	900.1413	0.5637	0.340	0.179	0.456
892.4836	0.9716	1.005	0.503	0.628	900.2805	0.5745	0.299	0.153	0.421
892.6228	0.9823	1.044	0.530	0.660	900.4198	0.5852	0.267	0.141	0.361
892.7620	0.9931	1.008	0.530	0.634	900.4894	0.5906	0.246	0.131	0.336
892.9011	0.0039	0.997	0.515	0.618	900.6287	0.6014	0.224	0.105	0.340
893.0404	0.0146	0.962	0.508	0.586	900.7638	0.6118	0.191	0.106	0.321
893.1796	0.0254	0.954	0.501	0.568	900.9027	0.6226	0.167	0.115	0.301
893.3187	0.0361	0.910	0.485	0.534	901.0416	0.6333	0.134	0.107	0.316
893.4580	0.0469	0.836	0.455	0.512	901.1820	0.6442	0.108	0.092	0.302
893.5972	0.0577	0.744	0.440	0.461	901.3216	0.6549	0.098	0.070	0.265
893.7364	0.0684	0.623	0.403	0.408	901.4605	0.6657	0.073	0.062	0.257
893.8757	0.0792	0.516	0.378	0.377	901.6006	0.6765	0.049	0.071	0.243
894.0148	0.0900	0.399	0.361	0.311	901.7395	0.6873	0.032	0.043	0.216
894.1540	0.1007	0.296	0.300	0.240	901.8784	0.6980	−0.004	0.023	0.197
894.2933	0.1115	0.232	0.262	0.208	902.0179	0.7088	0.005	0.014	0.184
894.4324	0.1223	0.205	0.237	0.169	902.1568	0.7195	−0.011	−0.001	0.176
894.5716	0.1330	0.170	0.210	0.166	902.2965	0.7303	−0.026	−0.015	0.177
894.7108	0.1438	0.122	0.190	0.142	902.4354	0.7411	−0.024	0.003	0.180
894.8500	0.1545	0.098	0.159	0.115	902.5742	0.7518	−0.021	0.000	0.171
894.9893	0.1653	0.057	0.127	0.076	902.7144	0.7626	−0.020	−0.002	0.161
895.1285	0.1761	0.013	0.105	0.053	902.8533	0.7734	−0.021	−0.003	0.149
895.2676	0.1868	−0.002	0.080	0.030	902.9922	0.7841	−0.032	−0.003	0.148
895.4069	0.1976	−0.015	0.066	0.041	903.2013	0.8003	−0.027	0.007	0.161
895.5461	0.2084	−0.027	0.039	0.042	903.3415	0.8111	−0.000	0.033	0.178
895.6853	0.2191	−0.044	0.025	0.033	903.4804	0.8219	0.005	0.048	0.194
895.8246	0.2299	−0.038	0.019	0.019	903.6193	0.8326	0.020	0.067	0.192
895.9639	0.2407	−0.051	0.010	0.038	903.7596	0.8435	0.025	0.091	0.168
896.1029	0.2514	−0.034	0.022	0.072	903.8978	0.8541	0.049	0.117	0.222
896.2422	0.2622	−0.024	0.031	0.088	904.0367	0.8649	0.086	0.152	0.256
896.3815	0.2730	−0.017	0.036	0.098	904.1756	0.8756	0.110	0.177	0.259
896.5207	0.2837	−0.024	0.024	0.080	904.3152	0.8864	0.164	0.214	0.286
896.6599	0.2945	−0.033	0.011	0.077	904.4554	0.8973	0.226	0.271	0.344
896.7992	0.3053	−0.024	0.009	0.095					
896.9384	0.3160	0.007	0.035	0.126					

TABLE II

Filters used in OAO-2 photometry

λ (Å)*	Filter Designation†	Halfwidth (Å)	$f_{\lambda 0}$ (m_λ=0, 0)**
3320	ST1F1	520	3.17×10^{-10} erg cm^{-2} s^{-1} $Å^{-1}$ ± 0.03
2980	ST1F4	410	3.22 ± 0.09
2460	ST3F2	360	3.28 ± 0.09
1910	ST3F1	260	6.47 ± 0.12
1550	ST4F1	270	5.88 ± 0.30
1430	ST4F3	240	6.88 ± 0.60

* Effective wavelength for flat spectrum.
† Instrument (ST=stellar photometer, F=filter) designation from Code *et al.* (1970).
** Errors estimated from filter degradation curve.

Table 3Ha

SWP HI DISPERSION
BINCENTER: 1250 A BINWIDTH 10 A

IDNUM	JD +2,440,000	PHASE	FLUX	mag
17769	5207.61	0.580967	4.833379e-10	0.057297
21429	5640.68	0.059297	3.861166e-10	0.301128
21430	5640.73	0.063162	3.827854e-10	0.310536
21433	5640.93	0.078623	3.662083e-10	0.358604
21447	5642.96	0.235553	4.576684e-10	0.116547
21448	5642.98	0.237099	4.448545e-10	0.147380
21467	5645.89	0.462056	3.456962e-10	0.421188
21469	5645.98	0.469014	2.909427e-10	0.608406
23787	5939.07	0.126174	4.350071e-10	0.171684
24359	6004.95	0.218942	4.906408e-10	0.041015
26601	6290.91	0.324266	4.414147e-10	0.155808
26602	6290.95	0.327358	4.202227e-10	0.209226
26609	6292.99	0.485055	3.109289e-10	0.536272
26612	6293.17	0.498970	3.048771e-10	0.557613
26613	6293.20	0.501289	3.233786e-10	0.493646
35692	7592.51	0.938541	3.586014e-10	0.381395
35693	7592.56	0.942406	3.465454e-10	0.418524
35705	7593.52	0.016611	3.681862e-10	0.352756
35706	7593.55	0.018930	3.639015e-10	0.365465
35720	7594.53	0.094681	3.275001e-10	0.479896
35721	7594.55	0.096227	4.015536e-10	0.258566
35757	7598.50	0.401553	3.864522e-10	0.300185
35758	7598.53	0.403872	3.881859e-10	0.295325
35760	7598.61	0.410056	3.958971e-10	0.273969
35762	7599.50	0.478851	3.211865e-10	0.501031
35763	7599.52	0.480397	3.195295e-10	0.506647
35765	7599.60	0.486580	3.272874e-10	0.480601
35784	7601.49	0.632673	4.811060e-10	0.062322
35785	7601.52	0.634992	4.810077e-10	0.062544
35787	7601.60	0.641176	4.912263e-10	0.039720
35794	7602.50	0.710743	4.845406e-10	0.054599
35795	7602.52	0.712289	4.646885e-10	0.100020
35797	7602.60	0.718473	5.095301e-10	0.000000
35803	7603.47	0.785722	4.843670e-10	0.054988
35804	7603.49	0.787268	4.980129e-10	0.024823
35806	7603.57	0.793452	5.054341e-10	0.008763
35810	7604.49	0.864565	4.184193e-10	0.213895
35811	7604.52	0.866884	4.396903e-10	0.160057
35813	7604.61	0.873841	4.325980e-10	0.177713
35818	7605.50	0.942636	2.813549e-10	0.644788
35819	7605.54	0.945728	3.343795e-10	0.457325
35821	7605.61	0.951139	3.256773e-10	0.485956
35828	7606.49	0.019160	2.960352e-10	0.589566
35829	7606.53	0.022252	3.342475e-10	0.457754
35831	7606.60	0.027663	3.536957e-10	0.396350
35836	7607.43	0.091820	3.423855e-10	0.431636

Table 3Hb

SWP HI DISPERSION
BINCENTER: 1365 A   BINWIDTH: 100 A

IDNUM	JD +2,440,000	PHASE	FLUX	mag
17769	5207.61	0.580967	5.800605e-10	0.106650
21429	5640.68	0.059297	4.413086e-10	0.403477
21430	5640.73	0.063162	3.772436e-10	0.573779
21433	5640.93	0.078623	4.974174e-10	0.273531
21448	5642.98	0.237099	5.953062e-10	0.078482
21467	5645.89	0.462056	3.768380e-10	0.574947
21469	5645.98	0.469014	3.758311e-10	0.577852
23787	5939.07	0.126174	5.234315e-10	0.218184
24359	6004.95	0.218942	6.194809e-10	0.035263
26601	6290.91	0.324266	5.486213e-10	0.167152
26602	6290.95	0.327358	5.475906e-10	0.169193
26609	6292.99	0.485055	3.863625e-10	0.547846
26612	6293.17	0.498970	3.852351e-10	0.551019
26613	6293.20	0.501289	3.602804e-10	0.623732
35692	7592.51	0.938541	4.481101e-10	0.386872
35693	7592.56	0.942406	4.436488e-10	0.397735
35705	7593.52	0.016611	4.302409e-10	0.431054
35706	7593.55	0.018930	4.359477e-10	0.416747
35720	7594.53	0.094681	5.215007e-10	0.222196
35721	7594.55	0.096227	5.487685e-10	0.166860
35757	7598.50	0.401553	4.868110e-10	0.296932
35758	7598.53	0.403872	4.980535e-10	0.272143
35760	7598.61	0.410056	4.629162e-10	0.351577
35762	7599.50	0.478851	3.889280e-10	0.540660
35763	7599.52	0.480397	4.003176e-10	0.509322
35765	7599.60	0.486580	3.810342e-10	0.562923
35784	7601.49	0.632673	5.554512e-10	0.153719
35785	7601.52	0.634992	5.601856e-10	0.144504
35787	7601.60	0.641176	5.143767e-10	0.237130
35794	7602.50	0.710743	5.960156e-10	0.077189
35795	7602.52	0.712289	6.113126e-10	0.049675
35797	7602.60	0.718473	5.593128e-10	0.146196
35803	7603.47	0.785722	6.290149e-10	0.018681
35804	7603.49	0.787268	6.399313e-10	0.000000
35806	7603.57	0.793452	5.967057e-10	0.075932
35810	7604.49	0.864565	5.490344e-10	0.166334
35811	7604.52	0.866884	5.518913e-10	0.160700
35813	7604.61	0.873841	4.968874e-10	0.274688
35818	7605.50	0.942636	4.299333e-10	0.431831
35819	7605.54	0.945728	4.211517e-10	0.454237
35821	7605.61	0.951139	3.587156e-10	0.628458
35828	7606.49	0.019160	4.220110e-10	0.452024
35829	7606.53	0.022252	4.280774e-10	0.436528
35831	7606.60	0.027663	3.856438e-10	0.549868
35836	7607.43	0.091820	5.067399e-10	0.253371
35837	7607.46	0.094139	5.186034e-10	0.228245

Table 3Hc

SWP HI DISPERSION
BINCENTER: 1430 A   BINWIDTH: 100 A

IDNUM	JD +2,440,000	PHASE	FLUX	mag
17769	5207.61	0.580967	5.368605e-10	0.132299
21429	5640.68	0.059297	3.879706e-10	0.484956
21430	5640.73	0.063162	3.391454e-10	0.630988
21433	5640.93	0.078623	4.477133e-10	0.329453
21448	5642.98	0.237099	5.618218e-10	0.082956
21467	5645.89	0.462056	3.534459e-10	0.586145
21469	5645.98	0.469014	3.518414e-10	0.591085
23787	5939.07	0.126174	4.998988e-10	0.209747
24359	6004.95	0.218942	5.830514e-10	0.042685
26601	6290.91	0.324266	5.211006e-10	0.164649
26602	6290.95	0.327358	5.161030e-10	0.175112
26609	6292.99	0.485055	3.621437e-10	0.559750
26612	6293.17	0.498970	3.548317e-10	0.581897
26613	6293.20	0.501289	3.356532e-10	0.642226
35692	7592.51	0.938541	4.004505e-10	0.450580
35693	7592.56	0.942406	3.960924e-10	0.462461
35705	7593.52	0.016611	3.793726e-10	0.509288
35706	7593.55	0.018930	3.807991e-10	0.505213
35720	7594.53	0.094681	4.710145e-10	0.274367
35721	7594.55	0.096227	5.047004e-10	0.199368
35757	7598.50	0.401553	4.514557e-10	0.320415
35758	7598.53	0.403872	4.625570e-10	0.294039
35760	7598.61	0.410056	4.355507e-10	0.359356
35762	7599.50	0.478851	3.577652e-10	0.572957
35763	7599.52	0.480397	3.626730e-10	0.558165
35765	7599.60	0.486580	3.513568e-10	0.592582
35784	7601.49	0.632673	5.150261e-10	0.177379
35785	7601.52	0.634992	5.263807e-10	0.153703
35787	7601.60	0.641176	4.819680e-10	0.249407
35794	7602.50	0.710743	5.602551e-10	0.085988
35795	7602.52	0.712289	5.747551e-10	0.058245
35797	7602.60	0.718473	5.259200e-10	0.154653
35803	7603.47	0.785722	5.947256e-10	0.021161
35804	7603.49	0.787268	6.064305e-10	0.000000
35806	7603.57	0.793452	5.642842e-10	0.078207
35810	7604.49	0.864565	5.132321e-10	0.181168
35811	7604.52	0.866884	5.172535e-10	0.172694
35813	7604.61	0.873841	4.680632e-10	0.281191
35818	7605.50	0.942636	3.871389e-10	0.487286
35819	7605.54	0.945728	3.784460e-10	0.511943
35821	7605.61	0.951139	3.210564e-10	0.690499
35828	7606.49	0.019160	3.675233e-10	0.543740
35829	7606.53	0.022252	3.747719e-10	0.522535
35831	7606.60	0.027663	3.410083e-10	0.625040
35836	7607.43	0.091820	4.668631e-10	0.283979
35837	7607.46	0.094139	4.753714e-10	0.264370

Table 3Hd

SWP HI DISPERSION
BINCENTER: 1570 A   BINWIDTH: 100 A

IDNUM	JD +2,440,000	PHASE	FLUX	mag
17769	5207.61	0.580967	5.226020e-10	0.161578
21429	5640.68	0.059297	3.695995e-10	0.537678
21430	5640.73	0.063162	3.693983e-10	0.538269
21433	5640.93	0.078623	4.155999e-10	0.410318
21448	5642.98	0.237099	5.585193e-10	0.089410
21467	5645.89	0.462056	3.711277e-10	0.533198
21469	5645.98	0.469014	3.497124e-10	0.597729
23787	5939.07	0.126174	5.088637e-10	0.190502
24359	6004.95	0.218942	5.974938e-10	0.016172
26601	6290.91	0.324266	5.295427e-10	0.147254
26602	6290.95	0.327358	5.288477e-10	0.148680
26609	6292.99	0.485055	3.702358e-10	0.535810
26612	6293.17	0.498970	3.637408e-10	0.555026
26613	6293.20	0.501289	3.640333e-10	0.554153
35692	7592.51	0.938541	3.982093e-10	0.456728
35693	7592.56	0.942406	3.889741e-10	0.482204
35705	7593.52	0.016611	3.534406e-10	0.586215
35706	7593.55	0.018930	3.560197e-10	0.578321
35720	7594.53	0.094681	4.565602e-10	0.308261
35721	7594.55	0.096227	4.885589e-10	0.234714
35757	7598.50	0.401553	4.716699e-10	0.272911
35758	7598.53	0.403872	4.848733e-10	0.242935
35760	7598.61	0.410056	4.808743e-10	0.251927
35762	7599.50	0.478851	3.688519e-10	0.539876
35763	7599.52	0.480397	3.792393e-10	0.509723
35765	7599.60	0.486580	3.828812e-10	0.499346
35784	7601.49	0.632673	5.334195e-10	0.139334
35785	7601.52	0.634992	5.330218e-10	0.140144
35787	7601.60	0.641176	5.376006e-10	0.130857
35794	7602.50	0.710743	5.709615e-10	0.065489
35795	7602.52	0.712289	5.852138e-10	0.038719
35797	7602.60	0.718473	5.839677e-10	0.041034
35803	7603.47	0.785722	6.064604e-10	0.000000
35804	7603.49	0.787268	6.059621e-10	0.000892
35806	7603.57	0.793452	5.960001e-10	0.018890
35810	7604.49	0.864565	5.066633e-10	0.195208
35811	7604.52	0.866884	5.158023e-10	0.175798
35813	7604.61	0.873841	5.113096e-10	0.185296
35818	7605.50	0.942636	3.761857e-10	0.518500
35819	7605.54	0.945728	3.686784e-10	0.540387
35821	7605.61	0.951139	3.578365e-10	0.572794
35828	7606.49	0.019160	3.381864e-10	0.634116
35829	7606.53	0.022252	3.519919e-10	0.590674
35831	7606.60	0.027663	3.582671e-10	0.571489
35836	7607.43	0.091820	4.454494e-10	0.335010
35837	7607.46	0.094139	4.623245e-10	0.294639

ORIGINAL PAGE IS
OF POOR QUALITY

Table 3He

SWP HI DISPERSION
BINCENTER: 1726 A   BINWIDTH: 100 A

IDNUM	JD +2,440,000	PHASE	FLUX	mag
17769	5207.61	0.580967	5.697628e-10	0.143298
21429	5640.68	0.059297	3.770887e-10	0.591425
21430	5640.73	0.063162	3.570040e-10	0.650851
21433	5640.93	0.078623	4.179998e-10	0.479593
21448	5642.98	0.237099	5.624760e-10	0.157274
21467	5645.89	0.462056	4.367560e-10	0.431936
21469	5645.98	0.469014	4.331079e-10	0.441043
23787	5939.07	0.126174	4.793135e-10	0.330984
24359	6004.95	0.218942	6.052545e-10	0.077688
26601	6290.91	0.324266	5.523760e-10	0.176947
26602	6290.95	0.327358	5.618786e-10	0.158427
26609	6292.99	0.485055	4.523294e-10	0.393897
26612	6293.17	0.498970	4.641119e-10	0.365977
26613	6293.20	0.501289	4.396904e-10	0.424666
35692	7592.51	0.938541	4.178054e-10	0.480098
35693	7592.56	0.942406	4.104981e-10	0.499256
35705	7593.52	0.016611	3.836105e-10	0.572807
35706	7593.55	0.018930	3.890639e-10	0.557481
35720	7594.53	0.094681	4.546393e-10	0.388366
35721	7594.55	0.096227	4.758630e-10	0.338829
35757	7598.50	0.401553	5.529735e-10	0.175773
35758	7598.53	0.403872	5.543233e-10	0.173126
35760	7598.61	0.410056	5.359883e-10	0.209645
35762	7599.50	0.478851	4.828138e-10	0.323084
35763	7599.52	0.480397	4.871724e-10	0.313327
35765	7599.60	0.486580	4.734314e-10	0.344391
35784	7601.49	0.632673	6.088476e-10	0.071262
35785	7601.52	0.634992	5.963415e-10	0.093796
35787	7601.60	0.641176	5.790725e-10	0.125701
35794	7602.50	0.710743	6.379490e-10	0.020568
35795	7602.52	0.712289	6.392280e-10	0.018394
35797	7602.60	0.718473	6.090279e-10	0.070940
35803	7603.47	0.785722	6.501498e-10	0.000000
35804	7603.49	0.787268	6.472641e-10	0.004829
35806	7603.57	0.793452	6.244062e-10	0.043865
35810	7604.49	0.864565	5.391063e-10	0.203348
35811	7604.52	0.866884	5.377617e-10	0.206059
35813	7604.61	0.873841	5.143291e-10	0.254431
35818	7605.50	0.942636	3.948733e-10	0.541389
35819	7605.54	0.945728	3.926916e-10	0.547405
35821	7605.61	0.951139	3.761133e-10	0.594237
35828	7606.49	0.019160	3.747246e-10	0.598253
35829	7606.53	0.022252	3.782211e-10	0.588169
35831	7606.60	0.027663	3.763037e-10	0.593687
35836	7607.43	0.091820	4.406790e-10	0.422228
35837	7607.46	0.094139	4.487005e-10	0.402642

Table 3Hf

SWP HI DISPERSION
BINCENTER: 1835 A   BINWIDTH: 100 A

IDNUM	JD +2,440,000	PHASE	FLUX	mag
17769	5207.61	0.580967	6.139146e-10	0.097066
21433	5640.93	0.078623	4.422085e-10	0.453268
21448	5642.98	0.237099	5.940634e-10	0.132754
21469	5645.98	0.469014	4.967312e-10	0.327033
24359	6004.95	0.218942	6.061615e-10	0.110865
26602	6290.95	0.327358	6.084314e-10	0.106807
26612	6293.17	0.498970	5.199715e-10	0.277387
35692	7592.51	0.938541	4.469224e-10	0.441756
35693	7592.56	0.942406	4.386493e-10	0.462042
35705	7593.52	0.016611	4.062611e-10	0.545323
35706	7593.55	0.018930	4.005478e-10	0.560700
35720	7594.53	0.094681	4.835293e-10	0.356279
35721	7594.55	0.096227	4.855598e-10	0.351729
35757	7598.50	0.401553	6.039578e-10	0.114820
35758	7598.53	0.403872	5.871798e-10	0.145408
35762	7599.50	0.478851	5.376284e-10	0.241131
35784	7601.49	0.632673	6.509366e-10	0.033489
35794	7602.50	0.710743	6.661508e-10	0.008404
35795	7602.52	0.712289	6.602023e-10	0.018143
35803	7603.47	0.785722	6.713275e-10	0.000000
35810	7604.49	0.864565	5.667433e-10	0.183870
35818	7605.50	0.942636	4.257984e-10	0.494326
35828	7606.49	0.019160	3.999385e-10	0.562353
35836	7607.43	0.091820	4.680926e-10	0.391507

Table 3La

SWP LOW DISPERSION
BINCENTER: 1250 A   BINWIDTH: 10 A

IDNUM	JD +2,440,000	PHASE	FLUX	mag
3340	3826.75	0.828815	4.977873e-10	0.025315
4151	3909.11	0.196373	5.095631e-10	-0.000070
5781	4067.80	0.464676	3.324438e-10	0.463629
35722	7594.59	0.099319	4.023422e-10	0.256436
35759	7598.58	0.407737	3.515358e-10	0.403001
35764	7599.58	0.485034	2.645223e-10	0.711769
35786	7601.56	0.638084	4.196690e-10	0.210657
35796	7602.56	0.715381	4.626355e-10	0.104827
35805	7603.53	0.790360	4.814317e-10	0.061587
35812	7604.57	0.870749	3.862037e-10	0.300884
35838	7607.50	0.097231	3.754345e-10	0.331589

Table 3Lb

SWP LOW DISPERSION
BINCENTER: 1365 A   BINWIDTH: 100 A

IDNUM	JD +2,440,000	PHASE	FLUX	mag
3340	3826.75	0.828815	6.178717e-10	0.038087
4151	3909.11	0.196373	6.007516e-10	0.068596
5781	4067.80	0.464676	4.100218e-10	0.483316
35722	7594.59	0.099319	5.043683e-10	0.258464
35759	7598.58	0.407737	4.598501e-10	0.358793
35764	7599.58	0.485034	3.571483e-10	0.633212
35786	7601.56	0.638084	4.832731e-10	0.304852
35796	7602.56	0.715381	5.546061e-10	0.155372
35805	7603.53	0.790360	5.697015e-10	0.126215
35812	7604.57	0.870749	4.876081e-10	0.295156
35838	7607.50	0.097231	4.666373e-10	0.342885

Table 3Lc

SWP LOW DISPERSION
BINCENTER: 1430 A   BINWIDTH: 100 A

IDNUM	JD +2,440,000	PHASE	FLUX	mag
3340	3826.75	0.828815	5.908035e-10	0.028344
4151	3909.11	0.196373	5.759195e-10	0.056048
5781	4067.80	0.464676	3.833227e-10	0.498041
35722	7594.59	0.099319	4.580699e-10	0.304623
35759	7598.58	0.407737	4.258415e-10	0.383833
35764	7599.58	0.485034	3.324800e-10	0.652539
35786	7601.56	0.638084	4.554297e-10	0.310899
35796	7602.56	0.715381	5.297783e-10	0.146717
35805	7603.53	0.790360	5.459190e-10	0.114132
35812	7604.57	0.870749	4.593254e-10	0.301651
35838	7607.50	0.097231	4.269308e-10	0.381059

Table 3Ld

SWP LOW DISPERSION
BINCENTER: 1570 A BINWIDTH: 100 A

IDNUM	JD +2,440,000	PHASE	FLUX	mag
3340	3826.75	0.828815	6.025151e-10	0.007086
4151	3909.11	0.196373	6.041017e-10	0.004230
5781	4067.80	0.464676	3.875810e-10	0.486100
35722	7594.59	0.099319	4.643580e-10	0.289874
35759	7598.58	0.407737	4.509264e-10	0.321742
35764	7599.58	0.485034	3.480424e-10	0.602926
35786	7601.56	0.638084	5.039351e-10	0.201070
35796	7602.56	0.715381	5.511954e-10	0.103742
35805	7603.53	0.790360	5.491769e-10	0.107725
35812	7604.57	0.870749	4.731564e-10	0.269494
35838	7607.50	0.097231	4.433966e-10	0.340025

Table 3Le

SWP LOW DISPERSION
BINCENTER: 1726 A   BINWIDTH: 100 A

IDNUM	JD +2,440,000	PHASE	FLUX	mag
3340	3826.75	0.828815	6.789924e-10	-0.047128
4151	3909.11	0.196373	6.295065e-10	0.035033
5781	4067.80	0.464676	5.122539e-10	0.258820
35722	7594.59	0.099319	4.496322e-10	0.400390
35759	7598.58	0.407737	5.237787e-10	0.234664
35764	7599.58	0.485034	4.465872e-10	0.407768
35786	7601.56	0.638084	5.587526e-10	0.164485
35796	7602.56	0.715381	6.077318e-10	0.073253
35805	7603.53	0.790360	5.955585e-10	0.095222
35812	7604.57	0.870749	4.849122e-10	0.318376
35838	7607.50	0.097231	4.185639e-10	0.478129

Table 3Lf

SWP LOW DISPERSION
BINCENTER: 1835 A   BINWIDTH: 100 A

IDNUM	JD +2,440,000	PHASE	FLUX	mag
3340	3826.75	0.828815	6.013175e-10	0.119576
4151	3909.11	0.196373	6.241562e-10	0.079102
5781	4067.80	0.464676	5.473110e-10	0.221751
35722	7594.59	0.099319	4.711889e-10	0.384348
35759	7598.58	0.407737	5.338869e-10	0.248713
35764	7599.58	0.485034	5.019627e-10	0.315657
35786	7601.56	0.638084	5.753888e-10	0.167433
35796	7602.56	0.715381	6.144736e-10	0.096078
35805	7603.53	0.790360	6.069353e-10	0.109480
35812	7604.57	0.870749	5.212308e-10	0.274761
35838	7607.50	0.097231	4.513677e-10	0.431010

Table 4a

LWP HI DISPERSION
BINCENTER: 2180 A   BINWIDTH: 100 A

IDNUM	JD +2,440,000	PHASE	FLUX	mag
2195	5640.74	0.063688	2.596501e-10	0.644246
2215	5642.96	0.235700	4.444409e-10	0.060682
2239	5645.89	0.462141	3.294622e-10	0.385704
2240	5645.95	0.466749	3.237564e-10	0.404672
4083	5939.08	0.126722	3.563230e-10	0.300608
4661	6001.02	0.914876	3.375665e-10	0.359319
4685	6004.95	0.219220	4.699883e-10	0.000000
6650	6290.90	0.323563	4.601679e-10	0.022926
6651	6290.95	0.327188	4.478099e-10	0.052483
6668	6292.99	0.485071	3.384279e-10	0.356552
6671	6293.17	0.498661	3.385957e-10	0.356014
15145	7592.52	0.939167	2.698284e-10	0.602498
15147	7593.53	0.017105	2.437854e-10	0.712698
15155	7594.53	0.095006	3.214753e-10	0.412349
15177	7598.51	0.402040	3.848717e-10	0.216928
15193	7599.50	0.478696	3.205718e-10	0.415404
15200	7601.52	0.635255	4.277210e-10	0.102316
15206	7602.50	0.710519	4.468301e-10	0.054861
15213	7603.47	0.786000	4.683034e-10	0.038993
15218	7604.50	0.865184	3.859452e-10	0.213904
15223	7605.50	0.942860	2.347521e-10	0.753694
15230	7606.50	0.019593	2.165310e-10	0.841417
15234	7607.46	0.094170	2.875005e-10	0.533621

Table 4b

LWP HI DISPERSION
BINCENTER: 2470 A BINWIDTH: 100 A

IDNUM	JD +2,440,000	PHASE	FLUX	mag
2195	5640.74	0.063688	1.607872e-10	0.868504
2215	5642.96	0.235700	3.344233e-10	0.073391
2239	5645.89	0.462141	2.233747e-10	0.511548
2240	5645.95	0.466749	2.218941e-10	0.518768
4083	5939.08	0.126722	2.680233e-10	0.313701
4661	6001.02	0.914876	2.314360e-10	0.473055
4685	6004.95	0.219220	3.566790e-10	0.003438
6650	6290.90	0.323563	3.356337e-10	0.069468
6651	6290.95	0.327188	3.336645e-10	0.075857
6668	6292.99	0.485071	2.259595e-10	0.499056
6671	6293.17	0.498661	2.262217e-10	0.497797
15145	7592.52	0.939167	1.824346e-10	0.731365
15147	7593.53	0.017105	1.514031e-10	0.933796
15155	7594.53	0.095006	2.112931e-10	0.571919
15177	7598.51	0.402040	2.660333e-10	0.321793
15193	7599.50	0.478696	2.085493e-10	0.586111
15200	7601.52	0.635255	2.957816e-10	0.206705
15206	7602.50	0.710519	3.383661e-10	0.060665
15213	7603.47	0.786000	3.578105e-10	0.000000
15218	7604.50	0.865184	2.987499e-10	0.195863
15223	7605.50	0.942860	1.708240e-10	0.802760
15230	7606.50	0.019593	1.441216e-10	0.987310
15234	7607.46	0.094170	1.970792e-10	0.647531